Matthew Kaspar, Kathryn Brown, Jonathan D. Price, Brian Vauter, and Kashif Mahmud. Mapping groundwater infiltration in Karst using LIDAR at Natural Bridge Caverns, Texas. *Journal of Cave and Karst Studies*, v. 88, no. 3, p. 78-99. DOI: 10.4311/2025ES0109

MAPPING GROUNDWATER INFILTRATION IN KARST USING LIDAR AT NATURAL BRIDGE CAVERNS, TEXAS

Matthew Kaspar[1,2], Kathryn Brown[1], Jonathan D. Price[1], Brian Vauter[3], and Kashif Mahmud[1]

Abstract

The Trinity and Edwards Aquifers, two of the nine major groundwater systems in Texas, are significant sources of water in south-central Texas. The aquifers are primarily hosted in a network of fractured carbonate rock with substantial areas of cavernous porosity. This study used Light Detection and Ranging (LiDAR) to generate a three-dimensional point cloud in centimeter resolution to study water flow patterns within cavernous porosity. The research was conducted at Natural Bridge Caverns (NBC), a cave system northeast of San Antonio, Texas. The NBC cave system formed within Cretaceous carbonate rocks that host the Trinity and Edwards Aquifers. Our investigation focused on various spatial resolutions of LiDAR point cloud data to map and assess the size and spatial distribution of cave ceiling features (stalactites). The best spatial resolution to accurately identify and count stalactites, when compared to manual counts of stalactites, was established. Areas of specific flow types were classified using stalactite morphology and spatial distribution. Additionally, the effect of LiDAR distance from the cave ceiling/wall surface on the identification process was evaluated. We found that the number of LiDAR scans has a greater effect on data quality than scan distance. For the analysis of larger ceiling sections in various cave chambers, we established an optimal resolution of 10 mm (~0.39 in.). We established an optimal threshold of 97th percentile for stalactite identification and a threshold of 93rd percentile for flow classification. The flow classification based on stalactite morphological analysis shows that the Castle of the White Giants exhibits the highest amount of flow despite the chamber having the thickest overburden. The chamber also presents the greatest flow rate within the caverns.

INTRODUCTION

Aquifers, the underground layers of water-permeable rock and sediments, are crucial water resources. Karst aquifers supply 20%–25% of the water resources around the world (Ford and Williams, 2007). The Edwards (Balcones Fault Zone) Aquifer and the Trinity Aquifer, two of the nine major groundwater systems in Texas, are a significant source of water in south-central Texas. The Edwards and Trinity Aquifers are primarily hosted in Cretaceous limestones and dolostones (Gary, 2011; Clark and Morris, 2017).

The primary recharge of the Edwards Aquifer in south-central Texas (Fig. 1) is along the Balcones Fault Zone (BFZ) (Kastning, 1983). BFZ normal faulting initiated during the Late Oligocene and continued into the Early Miocene, increasing the hydraulic conductivity of the area (Barker et al., 1994). In Bexar County and adjacent regions, the Edwards Aquifer flows south by southeast before curving to flow from west to east (Shindel, 2019). Fault displacement reaches 305 m. Fault-enhanced fractures have formed large zones of cavernous porosity (Gary, 2011). Faulting produces interfacing between the Edwards and Trinity aquifers (Lindgren et al., 2004; George et al., 2011; Bruun et al., 2016).

The strata of the Trinity and Edwards Groups host numerous caverns. The assessment of groundwater movement through speleothems plays a significant role in estimating infiltration through karst environments. Several studies have shown that the size, location, and shape of stalactites have a profound influence on infiltration in the subsurface (Klimchouk et al., 2000; Ford and Williams, 2007; Mahmud et al., 2015). Therefore, understanding the factors can provide valuable insights into groundwater dynamics in karst environments similar to the Natural Bridge Caverns. Terrestrial LiDAR is increasingly utilized in high-resolution 3D modeling of cavernous karst formations (Bellian et al., 2005; Pringle et al., 2006); a single LiDAR scan collects hundreds of millions of coordinates that detail speleothem distribution in caves. Most knowledge of groundwater flow behavior and potential contamination has come from drilling and well observation, leaving our understanding underdeveloped. Drilling uses carbonic acid to dissolve away rock, altering the rock, and may lead to inaccuracies in mapping karst formations. Similarly, wells are complicated and expensive to make and maintain. Use of LiDAR in caves allows the study of karst without additional host rock deformation or alteration of aquifer flow paths.

The Natural Bridge Caverns (NBC) is a cave system located within the BFZ, northeast of San Antonio, Texas, placing it directly in the recharge zone of the Edwards Aquifer. NBC has two major sections, a southern section named the Hidden Passages and a northern section named the Discovery Passages, which is the focus of this study. Both sections cut the Glen Rose Formation (Trinity Group) and the Kainer Formation (Edwards Group) (Fig. 2), somewhat uniquely

[1]Kimbell School of Geosciences, Midwestern State University, Wichita Falls, Texas 76308
[2]National Cave and Karst Research Institute, 400-1 Cascades Ave., Carlsbad, New Mexico 88220
[3]Natural Bridge Caverns, 26495 Natural Bridge Caverns Road, San Antonio, Texas 78266

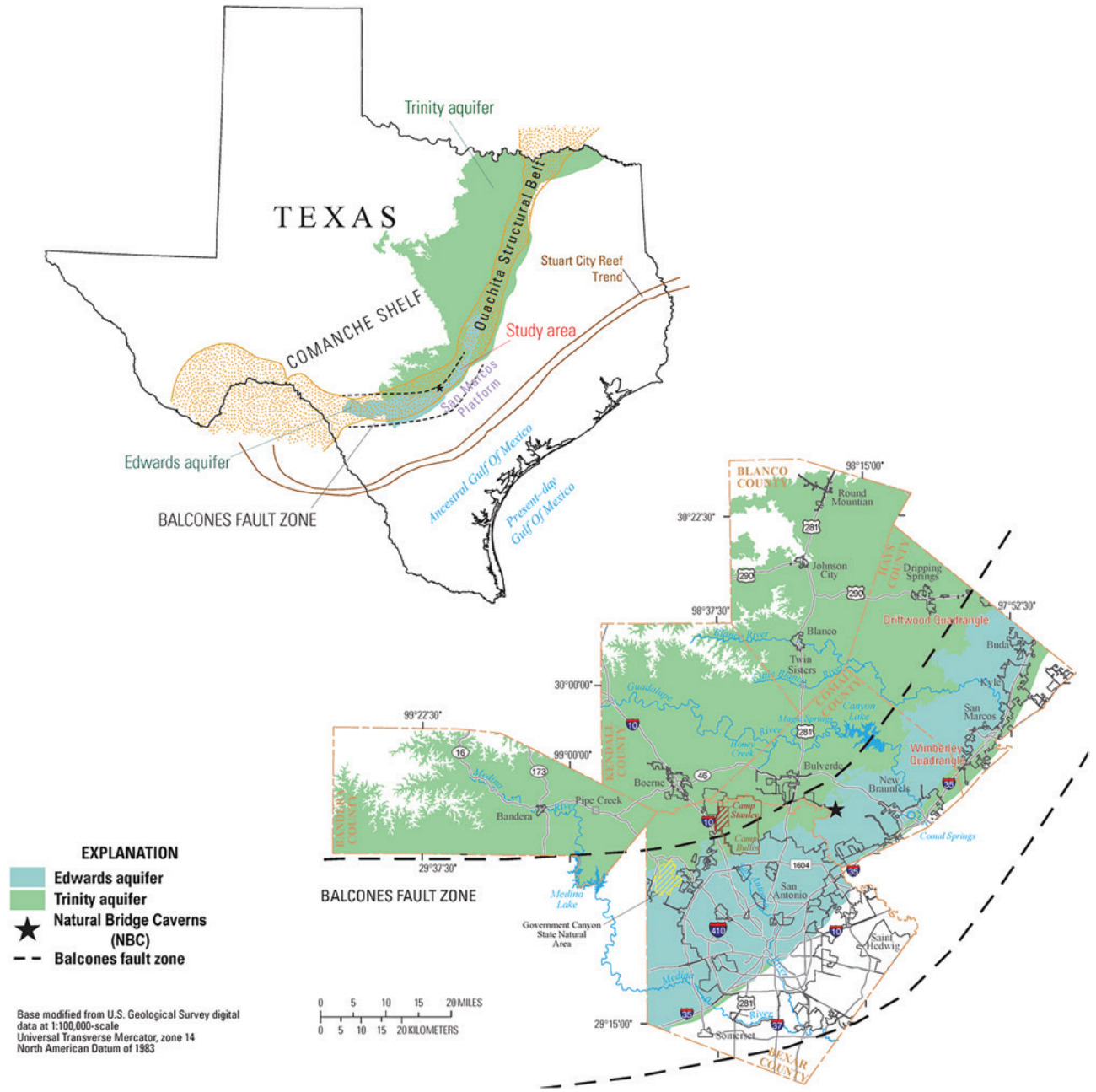


Figure 1. Location map showing the Edwards and Trinity Aquifers, the Balcones Fault Zone (BFZ), and Ouachita Structural Belt (top). Also, a close-up map of the Edwards Aquifer showing recharge zones of the BFZ and the location of NBC marked by the black star (bottom). Modified from Clark and Morris (2017).

connecting the two aquifers. The system is proximal to the saturated zone of the Trinity Aquifer; lower sections of NBC's Discovery Passages (the Castle of the White Giants and Purgatory Creek Sections) are prone to flooding events during intense precipitation (Gary, 2011).

The cavern system is hosted in the upper member of the Glen Rose Formation and the dolomitic and basal layers of the Kainer Formation, which are Lower Cretaceous sub-tidal to intertidal carbonates. The lower Glen Rose Formation is 91–98 m of rudist-reefal dolomitic limestone, highly karstified (Gary, 2011). The upper (Cavernous) member is roughly 152 m of interbedded dolomite and chalky limestone that weathers to stair-step morphology (Maclay and Small, 1986; Gary, 2011). Locally, the Glen Rose Formation is overlain by the nodular member of the Kainer Formation, 15–18 m of irregularly bedded micritic nodular limestone and clay. In the subsurface, it acts as a lower confining unit for the Edwards Aquifer but is karstified at the outcrop level (Gary, 2011). The cavern system roof partially extends into the dolomitic member, a dense crystalline carbonate with grainstone layers (Fig. 2).

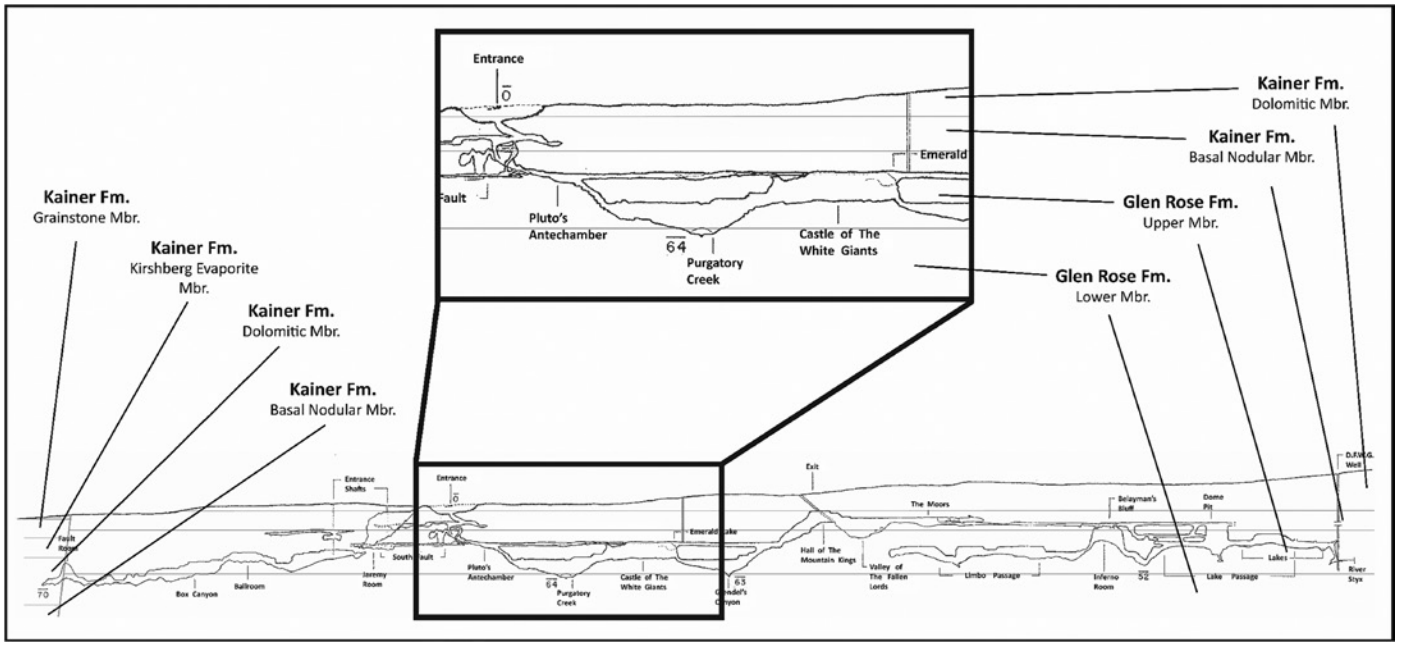


Figure 2. A cross section of NBC that shows the stratigraphic layers with which the cave system interacts within the Kainer Formation and the Glen Rose Formation modified from Kastning (1983) using information from Gary (2011).

Karst formation in the area occurred in two stages. First, exposure of the region subjected the strata to cavity formation by meteoric water shortly following deposition. The area was then buried, insulating it from further karstification. The next deformation of the area resulted in a 6° regional dip in present strata, causing extensional faulting and minor folding accompanied by fractures, which increased karst formation (Bellian et al., 2005; Clark and Morris, 2017).

Accessibility to aquifers is limited, which makes accurate data collection and modeling difficult. Most understanding of groundwater flow behavior and potential contamination has come from drilling and well observation, leaving our understanding underdeveloped. Drilling uses carbonic acid to dissolve away rock, altering the rock and leading to inaccuracies in mapping karst formations. Wells are also complicated and expensive to make and maintain. Studying caves gives access to key aquifer components and allows for the study of an aquifer without altering it.

This study applies the technique of Mahmud et al. (2015) to the recharge space of the Edwards and Trinity Aquifers. The objective of this study is to apply the technique in a more complex system at NBC. This method also needs parameter optimization based on a specific cave site and the associated stalactites' morphological attributes. NBC lies under an extremely heterogeneous karst environment. Hence, we optimize the algorithm parameters based on NBC stalactite morphology and spatial distribution, which are far more complicated than those in the previous study site at Mahmud et al. (2015). The initial results of Mahmud et al. (2015) were later validated using cave drip logger data in Mahmud et al. (2016), where cross-referencing outputs from both the stalactite morphological analysis and cave drip method showed correlating results. Here, we perform morphological and spatial analysis of cave ceiling features primarily using the cross-sectional area and aspect ratio of both singular and groups of stalactites to characterize the flow infiltration processes. The primary flow types defined are (1) intergranular percolation **matrix flow**, (2) conduit-focused **fracture flow**, and (3) matrix-and-fracture **combination flow**. This study identified the optimal resolution of LiDAR point clouds and input parameters that fit for analyzing the flow types at NBC. We evaluate scan attributes (such as distance, number, and angle) on the final stalactite count and flow classification using data from Brown et al. (2023).

METHODS

LiDAR Data Collection

This survey of NBC's Discovery Passages used a Leica BLK360 terrestrial LiDAR with a resolution of 5 mm at a distance of up to 45 m. The survey began at the Castle of the White Giants and scanned through the southern sections of the cave, including Purgatory Creek, Sherwood Forest, Pluto's Antechamber, and the south entrance of the cavern (Fig. 3). The survey collected 57 total individual scans. It attempted to scan most major speleothems from a minimum of four angles to maximize the quality of the LiDAR point cloud. Most of the accessible caverns (Purgatory Creek and switchbacks leading to Pluto's Antechamber) were limited to a single path, reducing the number of angles possible. Large areas, such as the Castle of the White Giants, allowed more scan angles. Once completed, the LiDAR data were

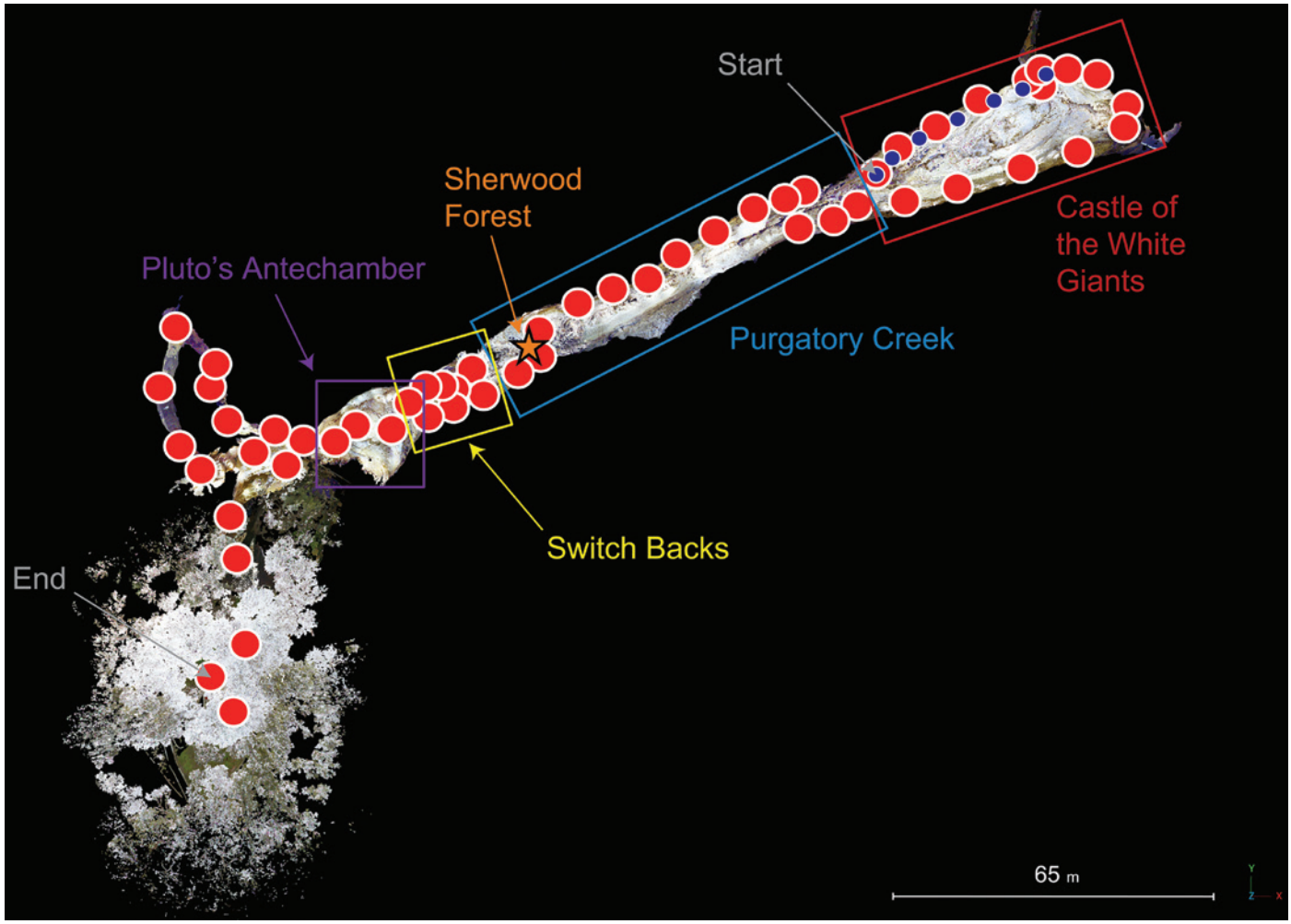


Figure 3. Final LiDAR point cloud of the Southern section of NBC's Discovery Passages showing all 57 scan locations represented by red dots from the start to end point covering the Castle of the White Giants, Purgatory Creek, Sherwood Forest, the Switch Back, and Pluto's Antechamber. Additional scans are considered from Brown et al. (2023) and are indicated by smaller blue dots.

downloaded using the Leica Cyclone REGISTER 360 software, where the individual scans were aligned and linked into a single point cloud to be exported. Combining multiple scans together fills in holes left by the individual scans and can further decrease point spacings by capturing stalactites at different angles and overlapping scans in existing areas.

The first LiDAR scan (set 1) of Discovery Passages was presented in Brown et al. (2023). This set started in the Castle of the White Giants and moved north to the exit passages. This was collected using the same LiDAR unit and scan strength as the later survey collected for this study.

Stalactite Identification Process

The study created an averaged surface to represent the overall cave ceiling topography using the moving average window of the ceiling surface. Window size was optimized through trial and error, varying the size in increments of 10 cm. The actual ceiling point cloud is subtracted from the smooth ceiling surface to generate a map of anomalies. These anomalies define the location of stalactites within the ceiling section. A histogram of the anomalies was plotted, and a threshold parameter was used to identify the individual stalactites. Anything below the threshold was natural rock surface variability and was not identified as stalactites. Lastly, a connected component analysis was performed (Mahmud et al., 2015) with the flow percentile threshold to group stalactites in close proximity for the identification of fracture and combination flow. The morphological properties of those groups determined the different water flow types. These properties consisted of stalactite's cross-sectional area and its aspect ratio. A more in-depth explanation is available in Mahmud et al. (2015).

Manual counts of stalactites are required for verification. This study counts these using photos of the cave ceiling and the point cloud viewed in CloudCompare. Total count assessment requires care to identify closely lying stalactites.

Visible spikes on cave ribbon are included in this count. Soda straws (subclass of matrix flow) are counted separately and subtracted from the total count to give the stalactite counts and soda straw counts as further comparison points.

Optimizing Resolution and Input Parameters

The technique introduced in Mahmud et al. (2015) is a semi-automated method that requires optimizing a set of input parameters for a specific cave site. These parameters are moving average window size, stalactite percentile threshold, and flow percentile threshold. The moving average window represents the cell numbers considered to generate the average ceiling surface. To optimize these parameters, the point spacing or resolution of the LiDAR point cloud must also be optimized to avoid extraneous data and to optimize the computational requirement. Four areas of easily identifiable features were clipped out of the ceiling point cloud using CloudCompare. Three of these were located in Purgatory Creek, and the remaining clip was from Sherwood Forest. These clips were cleaned of extraneous data points. The individual scans are then subsampled with six different point spacings or resolutions (2, 4, 6, 8, 10, and 12 mm). These clips are exported from CloudCompare and input into MATLAB to be converted into Stanford Geostatistical Modeling Software (SGEMS) files using the scattered interpolation prompt (scatteredInterpolant) with a natural neighbor interpolation method and no extrapolation method. The processed point clouds were analyzed to identify stalactite locations and generate flow type maps. Flow type maps were compared to a visual analysis of stalactite morphology to verify the accuracy with the input parameters. The tool also gives total stalactite counts of both soda straw stalactites and regular stalactites, which were compared to manual counts using field photographs and original LiDAR point clouds (Fig. 4). This was completed for every resolution with varying input parameters to find the optimum parameter set giving the closest stalactite counts.

Analyzing the Effect of Scan Number and Resolution on Stalactite Count

The northern section of NBC's Discovery Passages was surveyed as part of another study (set 1) (Brown et al., 2023). The previous survey area overlapped in the Castle of the White Giants. The major differences between the two surveys were the number of scans and the locations of the LiDAR. This survey consisted of 14 scans around the entire perimeter of the chamber, whereas the previous survey consisted of seven scans on one side of the chamber. The overlap permitted an evaluation of scan number, distance, and angle on the performance of the technique. Eleven clips (2 × 2 m) were cut out in the area both sets have in common (the upper path in Fig. 5C). Another eleven were cut out of the area exclusive to this study's survey (the lower path in Fig. 5C). These clips were run through the geometric analysis tool in CloudCompare to assess the surface volume of the point clouds in the area using a nearest neighbor input of

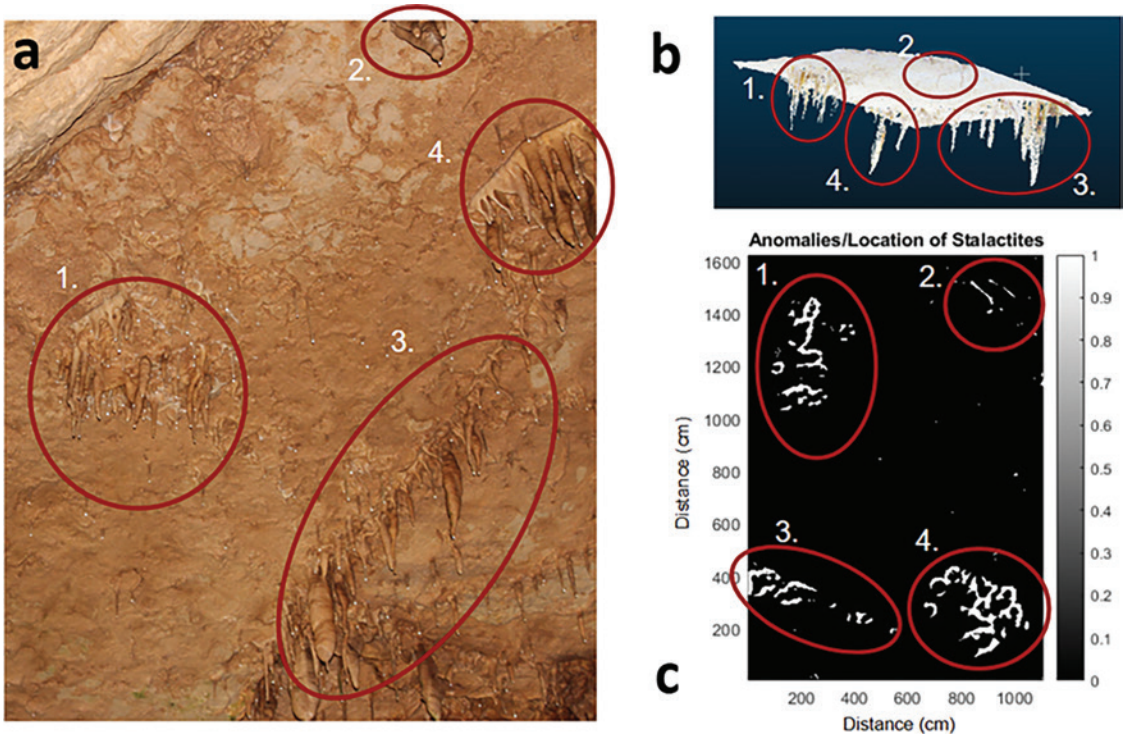


Figure 4. (a) Digital photograph and high-resolution LiDAR image (b) of a ceiling portion for the optimization and validation process. (c) Locations of individual stalactites identified using the morphological analysis located in Purgatory Creek section 2.

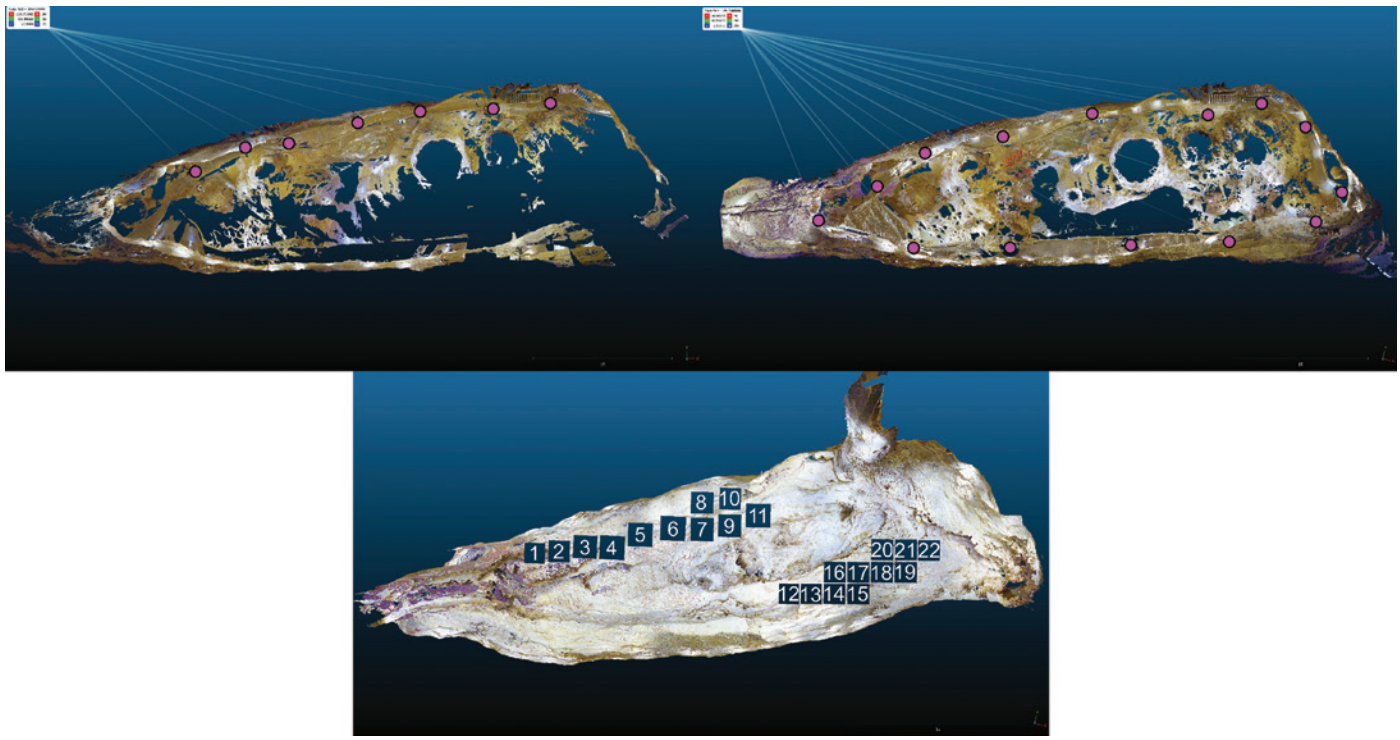


Figure 5. Point clouds of set 1 (a) and set 2 (b) in the Castle of the White Giants. The purple dots represent the location of LiDAR. All 22 clip sections are shown in (c).

1 unit (equivalent to 1 m). The statistics tool is then used on each clip to assess the mean surface density of each clip in points/m^2. This can then be converted to point spacing in millimeters using the equation edited from Heidmann (2018),

$$Point\ Spacing\left(mm\right)=1000\times\sqrt{\frac{1}{Point}Density\left(\frac{p}{m^2}\right)},$$

where point density is calculated as points per m^2.

Distance from the LiDAR location to the ceiling clips and the number of points in each clip can be determined in CloudCompare. The clips were cleaned and subsampled to the optimal resolution then exported to SGEMS files. SGEMS were analyzed to determine total stalactite counts for each clip. The differences between the distances to each clip, the resolution, the point counts, and the final stalactite counts were determined using Cloud Compare. We finally calculated the correlation coefficient for all of these attributes.

Flow Classification Analysis

After determining optimal parameters and resolution, large sections of Pluto's Antechamber and Purgatory Creek were clipped out and analyzed to determine the flow paths in those sections. The matrix flow, fracture flow, and combined flow categories were defined in Mahmud et al. (2015) as follows: Matrix flow is usually represented by smaller isolated stalactites in the cave ceiling. Soda straw stalactites were also included in the matrix flow category and were defined by lower stalactite diameter and higher length/diameter ratio. Stalactites having a cross-sectional area of <75 cm^2 and a connected component aspect ratio of <10 were identified as matrix flow, including the soda straws. Soda straws are defined by a diameter of <10 mm and a length/diameter ratio of >8. Pure fracture flow produces a linear distribution of ceiling stalactites. Stalactite groups with a large cross-sectional area (≥75 cm^2) and a large aspect ratio (>8:1) are identified as fracture flow. Lastly, combined flow forms larger stalactites with a more circular distribution. Stalactite groups with a large cross-sectional area (≥75 cm^2) but a low aspect ratio (<8:1) are identified as combined flow.

A large section containing several complex speleothems was clipped within the Castle of the White Giants for large-scale analysis (Fig. S1). This is along with the 22 sections analyzed in the previous section (Figure 5c) and provides a more complete picture of the flow classification in this chamber. Each of the new clips was cleaned and subsampled to the optimal resolution to analyze for flow classification.

RESULTS

Optimum Point Cloud Resolution

Manual count of stalactites for Purgatory Creek section 1 (Table 1) yielded 119 soda straws and 23 larger stalactites with a total of 142 stalactites. Purgatory Creek section 2 yielded 11 soda straws and 94 larger stalactites, a total of 105 stalactites. Purgatory Creek section 3 yielded 10 soda straws and 36 larger stalactites for a total of 46 stalactites. Sherwood Forest yielded 87 soda straw stalactites and 181 larger stalactites for a total of 268 stalactites.

In Purgatory Creek 2 and Purgatory Creek 3, total stalactite counts tend to decrease as resolution increases. In Purgatory Creek 1 and Sherwood Forest, the total count is largest at 4 mm resolution. When comparing total output stalactite counts in both Purgatory Creek section 1 and Sherwood Forest, considerably larger total stalactite counts were found across all resolutions than those found in visual counts (Table 1 and Fig. S2). When looking solely at soda straw counts, Purgatory Creek has a similar count to the manual count at 8 mm resolution, and Sherwood Forest matches its output count exactly to the manual count at 10 mm (Table 1 and Fig. S3). Large stalactite counts for Purgatory Creek section 1 and Sherwood Forest are still significantly larger than the manual counts at all resolutions. This generated a large difference in total stalactite count (Table 1 and Fig. S4). Stalactite counts for Purgatory Creek sections 2 and 3 were consistent across all resolutions and are most accurate to total stalactite counts at 10 mm (Table 2 and Fig. S3). For Purgatory Creek 3, the large stalactite counts matched the manual count exactly at both 6 and 10 mm. However, the large stalactite count for Purgatory Creek section 2 more closely matched the manual count at 10 mm (Table 1 and Fig. S4). The results determined that 10 mm is the optimal resolution for stalactite counts in this study area.

The moving average window size of 20 cm by 20 cm for the identification of stalactites was found to be optimal for NBC, compared to the 40 cm by 40 cm window used in Mahmud et al. (2015). A smaller window size provides more localized ceiling topography fluctuation, where larger window size results in a smoother surface. The larger window reduces the responsiveness to ceiling topography changes and results in inaccurate stalactite identification.

When verifying the accuracy of the combination of 10 mm resolution and the 97th stalactite percentile threshold of Mahmud et al. (2015), the clips were recompiled with different combinations of resolution and stalactite percentiles (Table 2). For Purgatory Creek 1 and Sherwood Forest, total stalactite counts remain significantly higher than manual counts, and the best match was found at the 97th percentile. Purgatory Creek 3 does match its total and manual counts at a resolution of 12 mm and a percentile of 98. At this combination, Purgatory Creek section 2 shows a difference of over 10 total stalactites and 3 soda straws. The final count is also off by more than 10 stalactites from the manual count for 8 mm, another combination where Purgatory Creek section 3 counts are close (Table 2). Due to the higher level of variance with other parameters, a 10 mm resolution and a threshold of 97th percentile were selected to be the optimal parameters for identifying stalactites at NBC (Fig. S5). To determine the optimal flow parameter, the clip was run with another set of varying thresholds to determine which threshold gave the most accurate flow patterns. When tested with the 95th percentile threshold, large portions of the stalactites are absent from the final flow paths. Lowering this to the

Table 1. Manual counts of stalactites vs automatic counts at different resolutions.

			Counts at Resolution (mm)					
Site Name	**Clip Size (m)**	**Manual Counts**	**2**	**4**	**6**	**8**	**10**	**12**
Soda Straws								
Purgatory Creek 1	2 × 2	119	159	161	124	117	85	62
Purgatory Creek 2	1 × 1.5	11	16	12	13	14	9	8
Purgatory Creek 3	1 × 0.6	10	13	12	13	8	7	6
Sherwood Forest	1 × 2	87	138	140	97	95	83	70
Large Stalactites								
Purgatory Creek 1	2 × 2	23	228	232	201	187	170	162
Purgatory Creek 2	1 × 1.5	94	123	123	107	118	96	108
Purgatory Creek 3	1 × 0.6	38	43	42	38	37	38	31
Sherwood Forest	1 × 2	181	302	308	264	251	276	240
Total Stalactites								
Purgatory Creek 1	2 × 2	142	387	393	325	304	255	224
Purgatory Creek 2	1 × 1.5	105	139	135	120	132	105	116
Purgatory Creek 3	1 × 0.6	48	56	54	51	45	45	37
Sherwood Forest	1 × 2	268	441	448	361	346	359	310

Note. All clips were run with a 97th stalactite percentile and a 93rd flow percentile.

Table 2. Stalactite counts at different stalactite percentiles.

Site Name and Resolution (mm)	Percentile			
	95th	96th	98th	99th
Soda Straw Counts				
Purgatory Creek 1 (8 mm)	95	96	156	192
Purgatory Creek 2 (8 mm)	14	14	12	17
Purgatory Creek 3 (8 mm)	10	9	10	7
Sherwood Forest (8 mm)	246	228	168	96
Purgatory Creek 1 (12 mm)	53	53	97	113
Purgatory Creek 2 (12 mm)	10	9	8	9
Purgatory Creek 3 (12 mm)	10	9	6	10
Sherwood Forest (12 mm)	188	180	150	209
Large Stalactite Counts				
Purgatory Creek 1 (8 mm)	220	202	192	160
Purgatory Creek 2 (8 mm)	194	139	79	56
Purgatory Creek 3 (8 mm)	56	40	37	30
Sherwood Forest (8 mm)	358	300	222	171
Purgatory Creek 1 (12 mm)	165	168	140	129
Purgatory Creek 2 (12 mm)	157	132	82	67
Purgatory Creek 3 (12 mm)	59	39	39	36
Sherwood Forest (12 mm)	305	270	204	172
Total Stalactite Counts				
Purgatory Creek 1 (8 mm)	315	298	348	352
Purgatory Creek 2 (8 mm)	208	153	91	73
Purgatory Creek 3 (8 mm)	66	49	47	37
Sherwood Forest (8 mm)	604	528	390	267
Purgatory Creek 1 (12 mm)	218	221	237	242
Purgatory Creek 2 (12 mm)	167	141	90	76
Purgatory Creek 3 (12 mm)	69	48	45	46
Sherwood Forest (12 mm)	493	450	354	381

93rd percentile corrects this, making this the optimal flow threshold (Figs. S5 and S6).

Relationship between Scan Number, Distance, and Final Counts

This study evaluated the effect of LiDAR scan distance from cave ceiling/walls and scan number on point cloud resolution and final stalactite counts by comparing set 1 (7 scans) to set 2 (14 scans) from the Castle of the White Giants (Fig. 5). The average distance increased for set 1 as we moved to the lower section of the Castle of the White Giants (sites 12–22), which was not covered in set 1. Set 2 has a lower point spacing (average of 4.4 mm) compared to set 1 (average of 5.6 mm), even in areas where set 1 was closer to the clipped area, although the spacing increased in the areas where distance increased. Point counts are higher in set 2 (Fig. S7c). The difference in point spacing does increase in the set with greater scan distances (Table 3 and Fig. S7b). The stalactite counts are larger for set 2 compared to set 1 (Fig. S7d). There is a moderate correlation between LiDAR scan distance and resolution with an R^2 of 0.454 (Fig. S8a). LiDAR scan distance and stalactite count have a weak linear to slightly negative trend with an R^2 of 0.091 (Fig. S8c). Point count and stalactite count have a weak linear negative trend with an R^2 of 0.044 (Fig. S8d). Lastly, LiDAR scan distance versus point count has a weak linear trend with an R^2 of 0.002 (Fig. S8b).

Flow Classification

The primary flow type present in Pluto's Antechamber is matrix flow (Fig. 6). There is a small amount of pure fracture flow and combined flow in Pluto's Antechamber #2 (Fig. 6). Purgatory Creek is mostly dominated by matrix flow, but large sections of fracture flow can be seen in clips Purgatory Creek #7 and Purgatory Creek #8 (Fig. 7). Small amounts of combined flow can also be seen in clips Purgatory Creek #1 and Purgatory Creek #7 (Fig. 7). The Castle of the White Giants consists of mostly fracture and combined flows, with a few patches of matrix flow present in the center of the chamber (Fig. 8). The large pillar in this section has been designated mostly as combined flow (Fig. 9). Considering the entire chamber, fracture flow tends to be located around the perimeter of the chamber, and the center is dominated by combined flow (Figs. 8 and 9). The flow types that represent the higher amount of water movement tend to be located in the deeper section of the caverns, with the shallower sections exhibiting almost entirely slower matrix flow.

DISCUSSION

The method used in Mahmud et al. (2015) is highly sensitive to three parameters that each depend on the morphology and spatial distribution of cave ceiling features. Parameter optimization is the first and most important step in the process because the cave features in NBC differ from those in Golgotha Cave, Western Australia (the study area of Mahmud et al., 2015). These two cave systems vary in size, morphology, age, petrology, climate, and speleothem density. All of these factors can impact how this technique detects stalactites, flow paths, and classification of flow types. NBC is in Cretaceous limestone and dolostone that has been deformed by normal faulting and associated stresses (Gary, 2011). The Golgotha Cave in Mahmud et al. (2015) is formed in Quaternary aeolianite (dune limestone). Lithology and age have significant impacts on cave morphology. The late Miocene faulting that promoted regional erosion and eventual NBC speleogenesis predates the Golgotha Cave by at least 5 million years. NBC's larger, more complex

Table 3. Differences between set 2 and set 1.

Clip #	Surface Density Difference	Resolution Difference (mm)	Distance Difference (m)	Point Count Difference	Soda Straw Difference	Stalactite Difference	Total Stall Difference
1	32880.578	1.017	0.266	241,862	328	447	775
2	15958.520	0.425	−0.357	−120 073	1654	508	2162
3	−11550.734	−0.252	−0.294	−224 358	36	−34	2
4	12564.570	0.568	−0.903	134,586	124	494	618
5	16773.016	0.665	−0.986	256,192	239	109	348
6	6482.945	0.383	−1.530	95,858	96	1309	1405
7	8910.230	0.493	−1.670	77,721	411	491	902
8	−14375.945	−0.278	−1.974	316,246	140	137	277
9	1038.957	0.046	−1.230	−343253	66	373	439
10	16367.500	0.699	−1.544	286,523	46	−6	40
11	−2587.805	−0.085	−1.614	−51974	23	128	151
12	23382.578	2.086	1.267	168,538	22	29	51
13	14896.408	1.384	2.804	75,489	7	268	275
14	11523.445	2.284	7.743	89235	−51	−42	−93
15	2742.477	0.466	8.005	38175	−48	−185	−233
16	20667.787	2.320	5.030	123633	−43	987	944
17	28884.367	2.965	5.191	184,086	11	384	395
18	25496.000	1.559	−0.513	201,724	83	130	213
19	21666.287	3.458	9.017	224034	−5	8	3
20	38105.457	1.258	−2.517	253,467	61	61	122
21	24131.461	0.875	−0.952	173,610	205	181	386
22	37159.783	2.511	1.039	223,500	85	83	168
Avg.	15050.813	1.129	1.103	110,219	159	266	425

Note. Locations of clip numbers can be seen in Figures 7 and 5c.

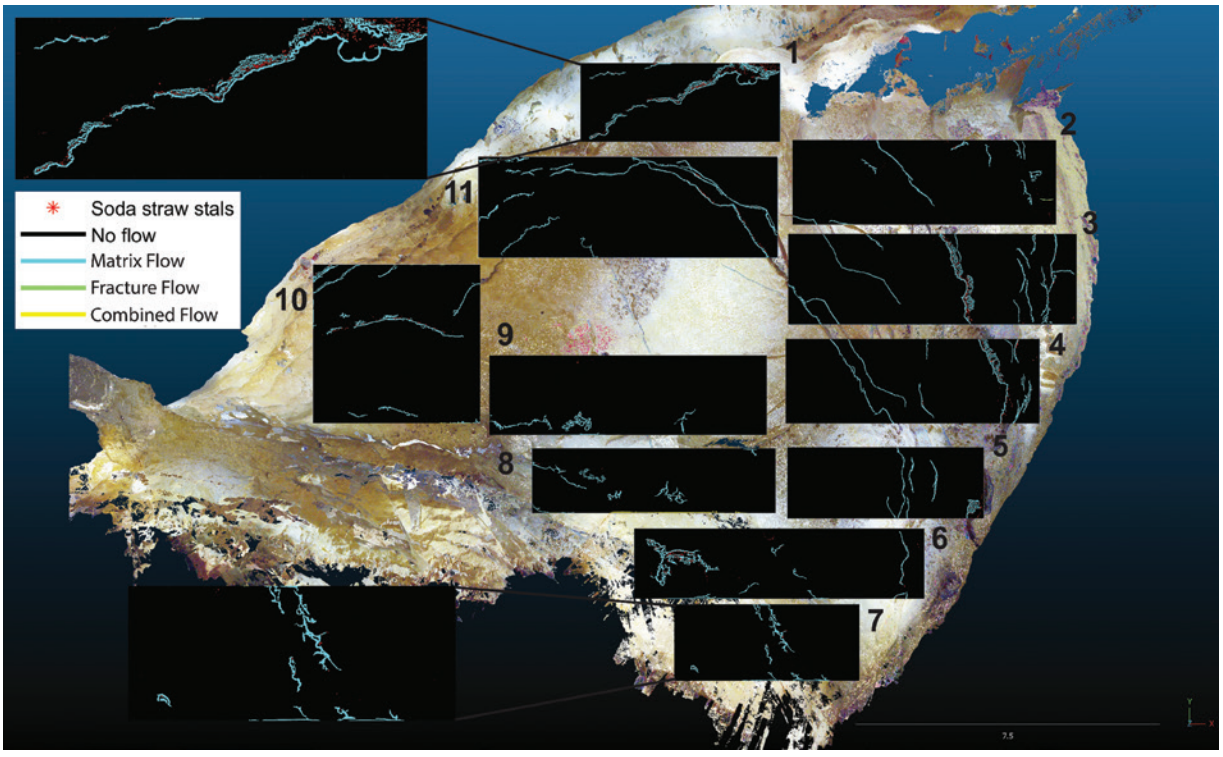


Figure 6. Flow classification maps of Pluto's Antechamber for all 11 clips, showing almost entirely matrix flow represented by blue and some soda straws represented by red asterisks. A small amount of fracture flow represented by green can be seen in clip #2.

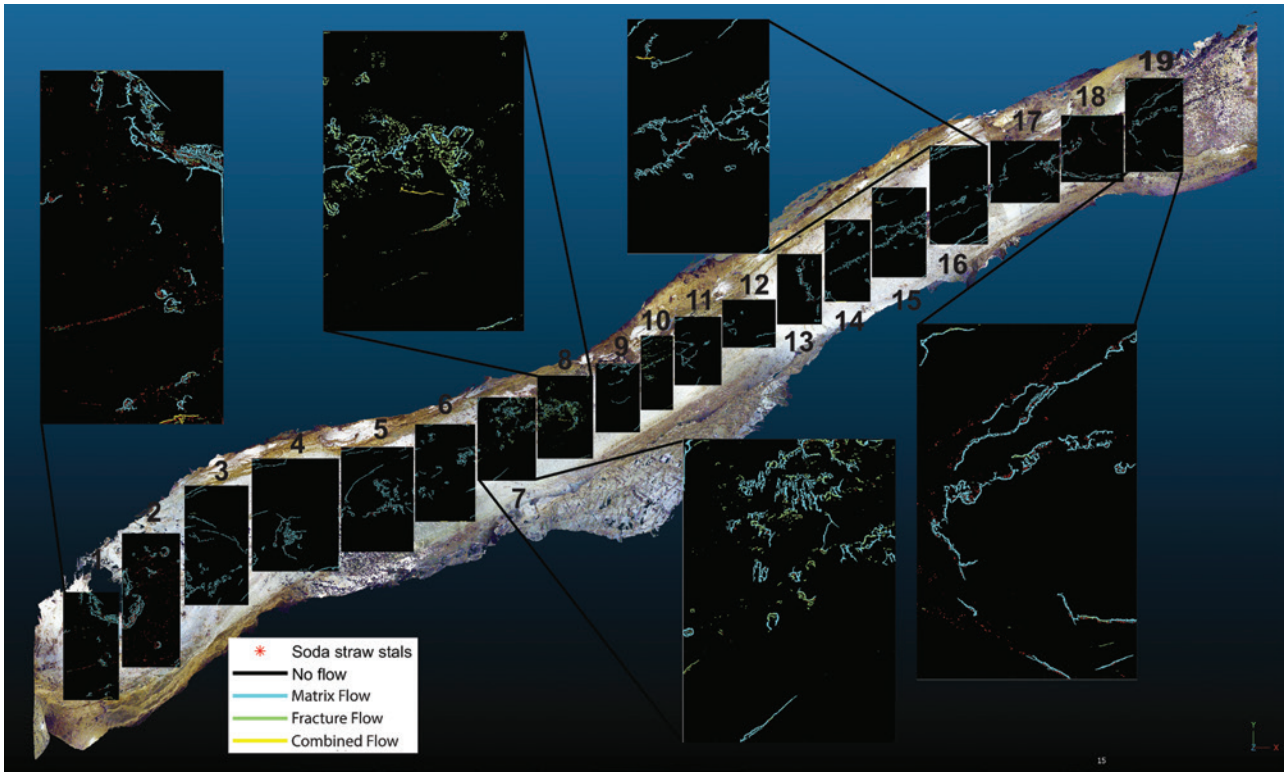


Figure 7. Flow classification maps of Purgatory Creek for all 19 clips showing mostly matrix flow in blue and fracture flow in green. A small amount of combined flow represented with yellow can be seen in clip #1.

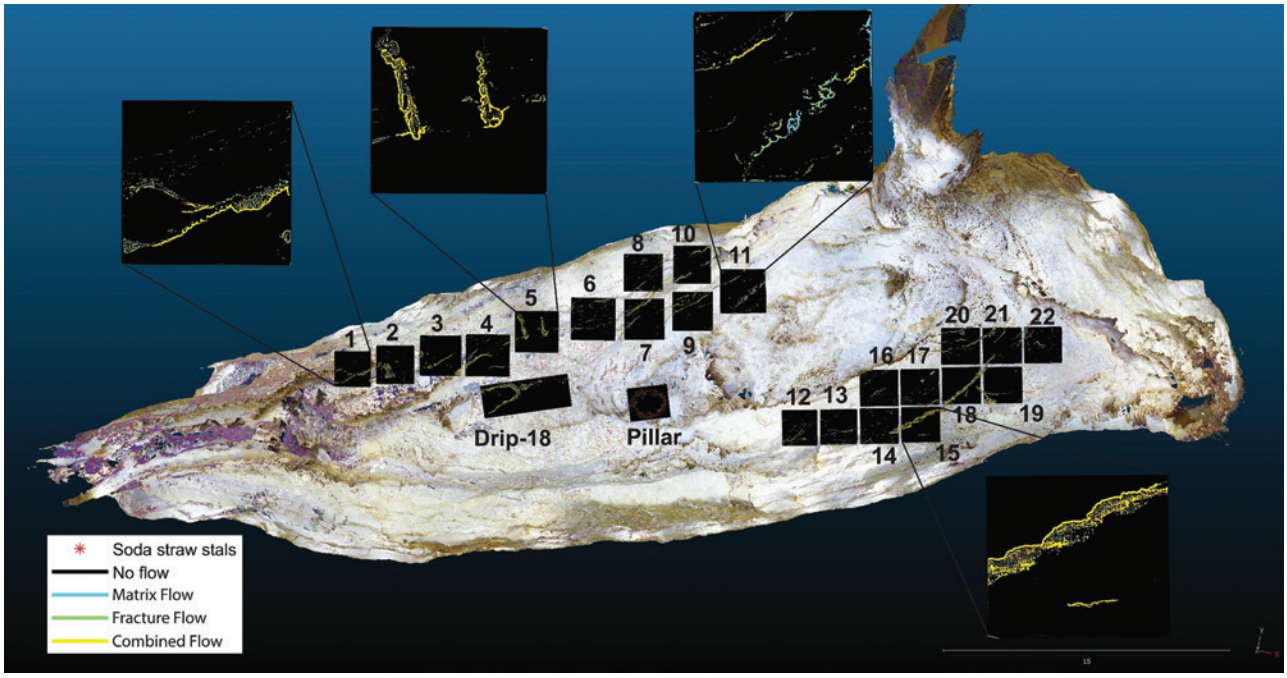


Figure 8. Flow classification maps of the 22 clips in the Castle of the White Giants plus one over drip logger 18 and the main pillar in the chamber. Flow types in the clips consist mostly of flow type 2 (fracture flow) represented by the color green and combined flow represented by the color yellow. A large number of soda straw stalactites were also detected, represented by red asterisks.

stalactites may be due in part to its antiquity, which allows for more opportunities for water flow and speleothem growth. The complexity of this system can also be attributed to two episodes of fracturing and meteoric water interactions, making the current and past movement of water more complex when compared to Golgotha Cave. Stalactites in NBC tend to be larger and cluster closely together, which introduces difficulty in optimizing parameters.

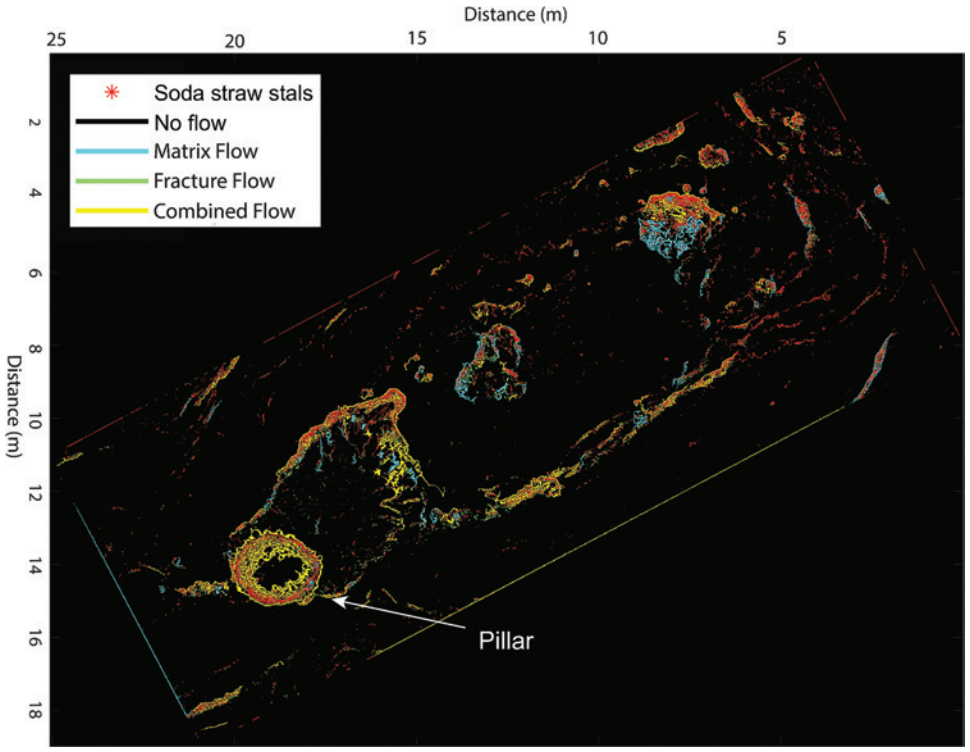


Figure 9. Large clip (9 × 24 m) of the Castle of the White Giants, which shows a very large number of soda straws represented by red asterisks, matrix flow represented by blue and combined flow represented by yellow.

In ceiling areas with larger stalactites, such as cave ribbons, both stalactite and soda straw counts are anomalously high. Purgatory Creek section 1 (Fig. S9, Table 1) examples this. While the method identifies a large number of stalactites, there are only 23 stalactites in the clip and most of the total stalactite count are soda straws (Table 1). The primary speleothem in this ceiling section is an area of cave ribbon (Fig. S9a). Most of the soda straws in this site are located in the center of the clip, away from the cave ribbon. The final flow map struggles to capture these soda straws (Fig. S9b). This is also seen in Sherwood Forest: this area is mostly composed of individual stalactites with no cave ribbon; however, we see an increase (from 181 to 276) in identified stalactites (Table 1). The soda straw locations tend to be more accurate, and the number of misidentified stalactites is sufficiently small, suggesting that individual stalactites are comparatively easier to capture than cave ribbons (Fig. S10).

The final interpolated point cloud representation of cave ribbons is problematic. When observing a 3D representation of the final point cloud, distinct artifacts are seen in the areas of cave ribbon (Figs. 10a and 10b). These artifacts are counted as many separate individual stalactites, increasing the total counts (Table 1). When observing the 3D representations of Purgatory Creek sections 2 and 3, we do not see these artifacts (Figs. 10c and 10d). There, the presence of distinct individual stalactites produces fewer artifacts and permits better identification of stalactites. This introduces extensive investigation when compared to Mahmud et al. (2015), as few cave ribbons were found in the tested areas of Golgotha Cave. It should also be noted that although these affect stalactite counts, their impact on flow identification is minimal. Flow identification groups the stalactites together and uses ratios between aspect ratio and cross-sectional areas of stalactite groups for identification (Mahmud et al., 2015). Due to these factors, it is recommended to perform parameter optimization in areas with smaller stalactites, as the complexity of the stalactites drives the inaccuracy in stalactite counts.

The optimized parameters found in Mahmud et al. (2015) for Golgotha Cave were a stalactite threshold of 97th percentile, a flow threshold of 94th percentile, and a moving average window of 40 cm by 40 cm. We found the same threshold (97th percentile) as the optimal value for stalactite identification in this cavern; however, the flow threshold was the 93rd percentile to capture flow classification accurately. The moving average window size used in this study is 20 cm by 20 cm. The smaller moving average captured more detailed local ceiling fluctuation compared to Mahmud et al. (2015).

Ultimately, there is no strong correlation between any of the point cloud properties and ceiling/wall distance from the LiDAR location. The one with the strongest correlation ($R^2 = 0.45$) is between resolution and distance, which indicates that resolution decreases with increasing distance between the object and LiDAR. There is scant correlation between distance and point count, distance and stalactite count, and point count and stalactite count.

Despite large parametric differences, there are areas shared by the two surveys (set 1 and set 2) where the stalactite count is dramatically different and others where it is statistically invariant. The two scan sets in Castle of the White Giants #5 differ by 348 total stalactites, whereas Castle of the White Giants #19 has a difference of only 3 total stalactites. This is likely due to the presence of LiDAR data voids, holes in LiDAR point clouds due to refraction, absorbance, or scattering of light or shadowing from interfering objects (Heidmann, 2018). When looking at the LiDAR point clouds for Castle of the White Giants #5 and Castle of the White Giants #19, significant data voids can be seen in Castle of the White Giants #5 from set 1 that are not present in set 2 (Fig. 11). These voids are not present in Castle of the White

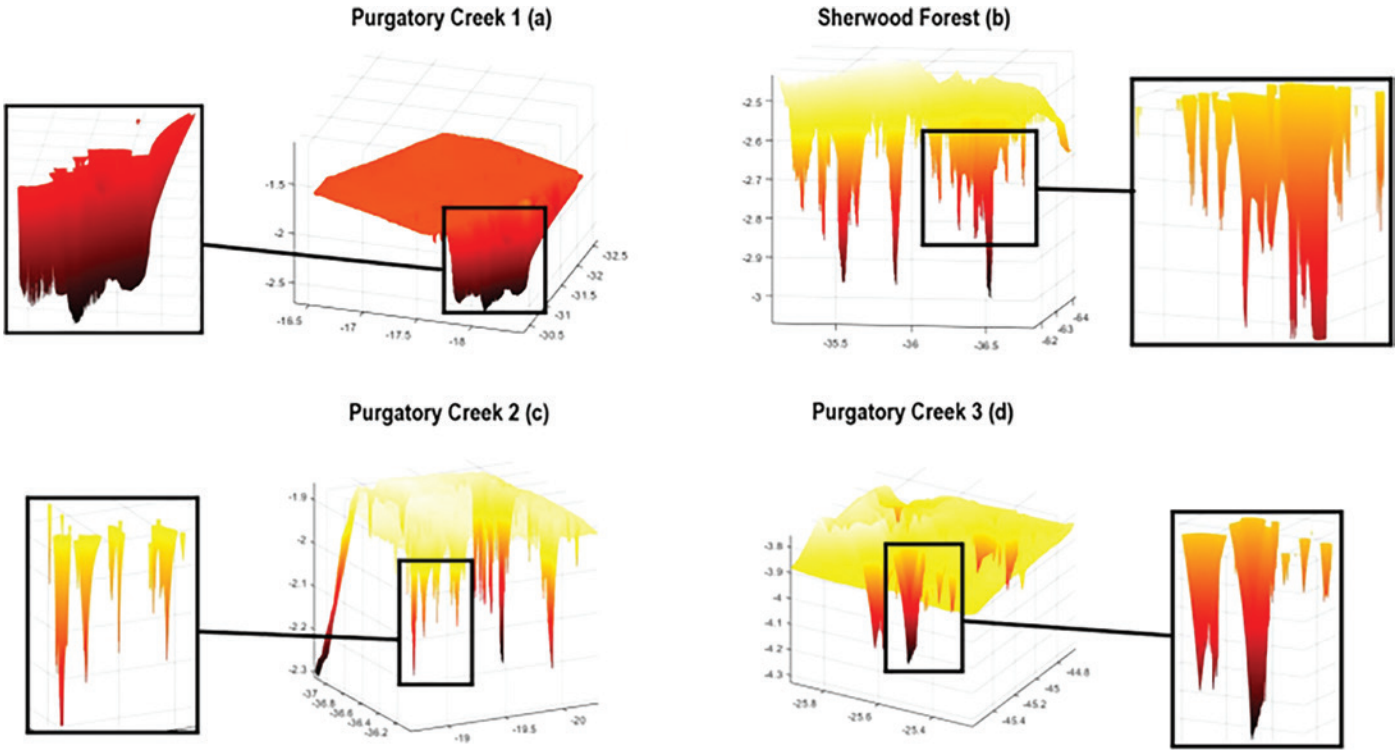


Figure 10. 3D representation of the ceiling for Purgatory Creek sections 1, 2, 3, and Sherwood Forest. Possible artifacts are marked by a black box and zoomed alongside in Purgatory Creek 1 (a) and Sherwood Forest (b). However, they are not present in Purgatory Creek 2 (c) and Purgatory Creek 3(d).

Giants #19 (Figs. 11b and 11e). The presence of these voids is likely due to the interference of the two large cave ribbons present in Castle of the White Giants #5 blocking the LiDAR's view in the affected areas (Fig. 11a). Having seven extra scans in set 2 compensated for those areas' absence on one side. This also explains the difference of over 2000 stalactites in Castle of the White Giants #2. It has a large data void that removes large sections of cave ribbon and stalactites that set 2 has intact (Figs. 11c and 11f). This highlights the importance of obtaining as many scans as possible when conducting a LiDAR survey inside a cave to minimize potential data gaps, hence improving final stalactite counts and producing accurate flow classification maps.

The flow classification maps in both Purgatory Creek and the Castle of the White Giants (Figs. 7 and 8) agree with the observations of the ceiling stalactites present in those two chambers. The Castle of the White Giants has mostly large complex groups of stalactites with large cross-sectional areas, classifying them as both fracture and combined flows (Fig. 8). This is also in agreement with work done in the Castle of the White Giants using drip logger data, where it was found that a majority of water infiltration in the chamber was due to combination flow (Remie et al., 2025). They used multidimensional scaling and agglomerative hierarchical clustering to classify similar drip types based on the drip loggers' time series and identify four unique drip regimes at those point locations within NBC, which are similar to our flow classification. Of the 5 drip loggers present from the Castle of the White Giants, 2 were identified as combination flow, 2 were classified as fracture flow, and the last one was classified as storage overburden flow (similar to soda straw flow in our classification scheme). Purgatory Creek has many more solitary stalactites with smaller cross-sectional areas (Fig. 7). Fracture and combination flow throughout the cavern tend to be located in the larger, deeper sections (Purgatory Creek and Castle of the White Giants). These sections cut through the upper member of the Glen Rose Formation. While matrix flow is present throughout the entire cavern, it is the only flow type to appear in the smaller chambers cutting through the shallower sections of the upper Glen Rose Formation (Pluto's Antechamber).

Overburden thickness remains consistent above both Pluto's Antechamber and Purgatory Creek and thickens over the Castle of the White Giants. Despite this, the Castle of the White Giants contains flow types representing the largest amount of water movement. This suggests that infiltration time in this system is controlled more by secondary porosity and less due to differences in overburden thickness. There are also no significant changes in stratigraphic units across the southern section, as there is only about a 2-degree dip in units with no changes in thickness, which leads to minimal impact from the rock units present. We identify that preexisting conduits are more developed above the Castle of the White Giants and the middle of Purgatory Creek, with other locations above Purgatory Creek and Pluto's Antechamber being less developed (Fig. 12). There is a solution fracture (NBS—38) located 60 m west of the cavern located near the

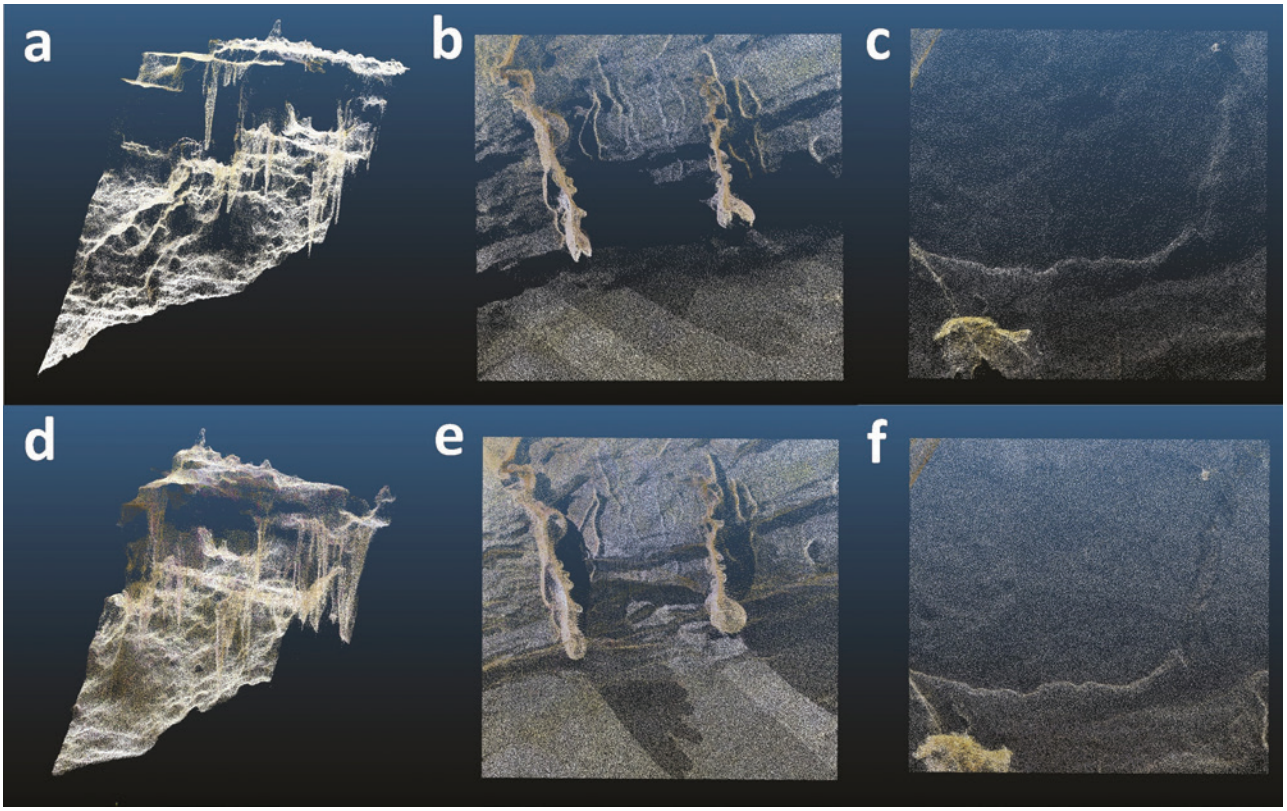


Figure 11. LiDAR point clouds showing the presence of data voids in different clips from the Castle of the White Giants (CWG): (a) showing CWG#2 from set 1, (b) showing CWG#5 from set 1, (c) showing CWG#19 from set 1, (d) showing CWG#2 from set 2, (e) showing CWG #5 from set 2, and (f) showing CWG#19 from set 2.

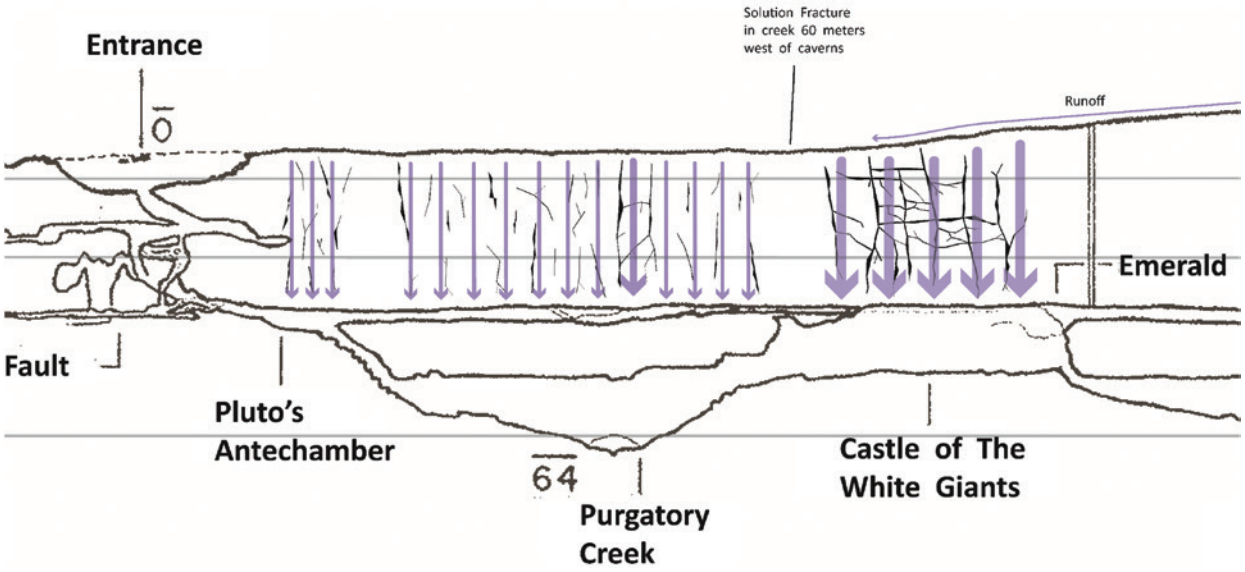


Figure 12. Conceptual framework of potential fracture distribution within the overburden rock layers above the southern section of NBC Discovery Passages. Water movement is represented by purple arrows, with thicker arrows representing higher estimated flow rates and thinner arrows representing lower. Also noted is the location of the solution fracture over the Castle of the White Giants, which serves as a point of water infiltration in the subsurface.

southern section of the Castle of the White Giants (Gary, 2011), which presumably act as an area for water to easily infiltrate in the below cave chamber. Also, an access shaft (NBS-55) above the Purgatory Creek dumps water after rain events straight to the chamber, impacting water availability for subsurface infiltration above this chamber and resulting in less stalactite development in recent years. Another factor to consider is topography's effect on runoff. Elevation

decreases as you move towards the south of the cave, leading to a severe drop in elevation near the entrance, with elevation rising after that. This potentially concentrates runoff in the southern section, leading to a higher quantity of infiltrating water in these sections. Historically, the entrance has been the primary point of water infiltration into the cave, supplying a large quantity of faster moving water to form thinner chambers, such as Purgatory Creek (Gary, 2011). This, however, has changed with the installation of doors that now block major water flow into the entrance section.

Few areas are identified as different flow types within different ceiling sizes. Purgatory Creek 1, for example, is identified as combined flow in the smaller optimization clip but identified as matrix flow in the larger clip, Purgatory Creek 16. The resolution and input parameters are unchanged, so not a likely cause of differences. It is possible that the larger clip simply provided more data for the method to use in identification. Alternatively, it is also possible that larger clips may introduce more error into the identification method.

We find that ceiling areas lacking stalactites are misidentified as matrix flow, for example, in Pluto's Antechamber (Fig. S11). This ceiling area actually has few stalactites, most of them being located along the margins of the chamber. Interbedded clay layers are common to the carbonate rock that hosts NBC, and these layers cause a distinctive stair-step terracing pattern on the ceiling throughout the cavern (Gary, 2011). These terraces are identified as matrix flow, even without the presence of stalactites (Fig. S11). The elevation of the terraces is likely being registered as an anomalous area and misidentified as stalactites.

Flow classification maps failed to identify the recent development of fracture flow. Numerous soda straws oriented along a potentially newly developed fracture at Fig. S9 did not register as fracture flow. These soda straws are too tiny to model them adequately. This can also affect the identification of younger stalactites along fractures, potentially leading to misidentification of matrix or no flow. Smaller stalactites can also lead to misidentification of flow types that represent less water movement.

This technique requires high processing power to run the algorithm and to process the LiDAR point clouds in Cloud Compare. Cloud Compare needs more RAM to render all data points and a faster CPU to calculate surface density. MATLAB also needs a faster CPU to run this algorithm, especially for larger study areas. A majority of the data processing for this study was performed using a computer with 128 GB of RAM and a Ryzen 7950× CPU, which contains 16 processing cores that run at a clock speed of 5.4 GHz. On average, the smaller clips took less than a minute to complete, but larger ceiling sections required 10 min. The large clip in the Castle of the White Giants with a dimension of 25 × 18 m ran 12 h and 35 min to complete. Comparing this to a computer with 256 GB of RAM and an Intel(R) Xeon(R) w5-3335x CPU, which also contains 16 processing cores but a slower clock speed of 3.1 GHz. This computer takes 19 h and 35 min to run the same clip. Hence, CPU clock speed has a greater impact on MATLAB processing, while RAM has a greater impact on LiDAR point cloud rendering.

CONCLUSIONS

Three-dimensional LiDAR surveys of caverns provide a useful tool to understand the preferential water movement in highly heterogeneous karst formations. Our results utilize cavern morphology, predict infiltration water movement, and discover areas of cavern development while leaving the aquifer unaltered.

Optimal parameters for the study of flow types exhibited by speleothems at NBC's Discovery Passages are a threshold of 97th percentile to identify stalactites, a threshold of 93rd percentile to classify flow types, and a 20 cm by 20 cm moving average window. The optimum thresholds are similar to those from prior efforts in cave LiDAR mapping of speleothems, but the optimum moving average window size is reduced to 50% for NBC compared to Golgotha cave (Mahmud et al., 2015). The optimization of input parameters must always be the first step in this method, as cave morphology varies significantly due to factors such as age, lithology, and preexisting structures.

The primary areas containing fracture and combined flows, hosting the most water movement through NBC, are located in the deeper sections of the cavern (Purgatory Creek and the Castle of the White Giants). Fracture flow in Purgatory Creek tends to be consolidated to one area (located in clips 7 and 8 in Fig. 7), with a small fraction of combination flow being present at the end closest to Sherwood Forest. Fracture flow in the Castle of the White Giants tends to be located closer to the walls of the chamber, with large amounts of combination flow being located in the center of the chamber (Fig. 8). This matches the methodology, as the stalactites with higher aspect ratio and cross section area are located more in Purgatory Creek and around the edge of the Castle of the White Giants. Lastly, the center of the Castle of the White Giants is dominated by more circular pillars, driven by combination flow. Areas with slow matrix flow are located in the shallower sections of the cave system (Pluto's Antechamber). Lithologically, fracture flow and combination flow tend to be located in the deeper sections of the cave that cut through the upper member of the Glen Rose Formation.

We estimate that the larger secondary porosity is distributed over the Castle of the White Giants, as we identify flow types representing a higher quantity of flow (combination and fracture) despite the greater overburden thickness. The secondary porosity over Purgatory Creek and Pluto's Antechamber is assumed to be less developed, as those cave ceilings are dominated by matrix flow.

When conducting a LiDAR survey in a cave, it is essential to collect as many scans as possible to avoid data voids in the point clouds. This methodology performed accurately in various ceiling sections within NBC's Discovery Passages; however, there were few caveats while analyzing larger cave ceilings with complex stalactite distributions. Larger stalactites and other ceiling features such as cave ribbons create anomalously large stalactite counts, challenging the optimization process. It is best to optimize input parameters in areas with smaller, simple ceiling sections. There was also anomalous flow classification produced due to the presence of terracing in the cavern, despite no stalactites being visible.

ACKNOWLEDGMENTS

The authors would like to acknowledge the thoughtful reviews of Steven Rosscoe and Andrew Katumwehe on an early draft. The authors acknowledge Elizabeth Elkins for her assistance in the LiDAR survey. Lastly, our sincere thanks to the staff of NBC for their help in the data collection process.

DATA AND CODE AVAILABILITY

The raw data and code used in this study are freely available from this Github repository: https://github.com/mtk7120/Methodology-for-the-Identification-of-Ground-Water-Flow-Types-in-Caverns-using-LiDAR-and-MATLAB-.git

REFERENCES

Barker, R. A., Bush, P. W. , and Baker, E. T. Jr., 1994, Geological history and hydrogeologic setting of the Edwards-Trinity aquifer system west-central Texas: U.S. Geological Survey, Water-Resource Investigations Report 94-4039, 51, p. 27–44, https://doi.org/10.3133/wri944039

Bellian, J., Kerans, C. , and Jennette, D. , 2005, Digital outcrop models: Applications of terrestrial scanning LiDAR technology in stratigraphic modeling: Journal of Sedimentary Research, v. **75**, no. 2, p. 166–176. https://doi.org/10.2110/jsr.2005.013

Brown, K., Mahmud, K., Katumwehe, A. B. , Price, J. D. , and B. Vauter, 2023, Morphological and spatial analysis of cave LiDAR remote sensing to identify karst water infiltration pathways: AGU23, San Francisco, California, 11–15 December, American Geophysical Union, H51P-1304.

Bruun, B., Jackson, K., Lake, P., and Walker, J., 2016, Texas aquifers study groundwater quantity, quality, flow, and contributions to surface water: Texas Water Development Board Report, p. 74–81, https://digitalcommons.usf.edu/kip_articles/4891.

Chang, C and Liu, L., 2021, Investigating the formation of the Cretaceous Western Interior Seaway using landscape evolution simulations: GSA Bulletin, v. **133**, no. 1–2, p. 347–361.

Clark, A. K and Morris, R. R., 2017, Bedrock geology and hydrostratigraphy of the Edwards and Trinity aquifers within the Driftwood and Wimberley 7.5-minute quadrangles, Hays and Comal Counties, Texas: U.S. Geological Survey Scientific Investigations Map 3386, 12, pp. 2–8, https://doi.org/10.3133/sim3386

Ford, D and Williams, P. D., 2007, *Karst Hydrogeology and Geomorphology*: Hoboken, NJ, USA, Wiley, 562 p.

Gary, M. O., 2011, *Geological Assessment for Natural Bridge Caverns Comal County*: Texas, Zara Environmental LLC, 40 p.

George, P. G., Mace, R. E., and Petrossian, R., 2011, Aquifers of Texas, Texas Water Development Board Report 380, 172 p, https://doi.org/10.3133/wri944039

Heidmann, H. K., 2018, Lidar Base Specification Version 1.3: United States Geological Survey, National Geospatial Program, Chapter 4 of Section B: U.S. Geological Survey Standards Book 11, Collection and Delineation of Spatial Data: p. 5–52, https://doi.org/10.3133/tm11b4.

Kastning, E. H., 1983, Geomorphology and hydrogeology of the Edwards Plateau Karst, Central Texas [Ph.D. thesis]: University of Texas at Austin, Texas Speleological Survey Reissue, 657 p., https://texasspeleologicalsurvey.org/PDF/Kastning.pdf.

Klimchouk, A. B., Ford, D. C., Palmer, A. N., and Dreybrodt, W., 2000, *Speleogenesis and Evolution of Karst Aquifers*: Huntsville, AL, USA, National Speleological Society, 514 p.

Lindgren, R. J., Dutton, A. R., Hovorka, S. D., Worthington, S. R. H., and Painter, S., 2004, Conceptualization and Simulation of the Edwards Aquifer, San Antonio Region, Texas: United States Geological Survey Scientific Investigations Report 2004-5277, p. 27–31.

Mahmud, K., Mariethoz, G., Pauline, C. T., and Baker, A., 2015, Terrestrial Lidar survey and morphological analysis to identify infiltration properties in the Tamala Limestone, Western Australia: IEEE Journal of Selected Topics in Applied Earth Observations and Remote Sensing, v. **8**, no. 10, p. 4871–4881.

Mahmud, K., Mariethoz, G., Baker, A., Treble, P. C., Markowska, M., and McGuire, E., 2016, Estimation of deep infiltrating unsaturated limestone environments using lidar and drip count data: Hydrology and Earth System Sciences, v. **20**, no. 1, p. 359–373.

Maclay, R. W and Small, T. A., 1986, Carbonate Geology and Hydrology of the Edwards Aquifer in the San Antonio Area: Texas: Texas Water Development Board Report, p. 13–28, https://digitalcommons.usf.edu/kip_articles/612/.

Pringle, J. K., Howell, J. A., Hodgetts, D., Westerman, A. R., and Hodgson, D. M., 2006, Virtual outcrop models of petroleum reservoir analogues: A review of the current state-of-the-art: First Break, v. **24**, no. 3, p. 33–42.

Remie, R., Mahmud, K., Gary, M., Price, J. D., Katumwehe, A., and Vauter, B., 2025, Using Cave Drip Loggers to Characterize Groundwater Infiltration and Examine Hydrological Response in Cretaceous Karst Formation: EGUsphere [preprint], https://doi.org/10.5194/egusphere-2025-2623.

Shindel, G. M., 2019, Genesis of the Edwards aquifer, *in* Sharp, J. M., Green, R. T., and Shindel G. M., eds., *The Edwards Aquifer: The Past, Present and Future of a Vital Water Resource*: Boulder Colorado, Geological Society of America Memoir, 215, p. 9–18. https://doi.org/10.1130/2019.1215(02).

USGS, 2021, Water Resource Mission Area, Principal Aquifers of the United States, United States Geological Survey: https://www.usgs.gov/mission-areas/water-resources/science/principal-aquifers-united-states (accessed April 28 2025).

Weary, D. J. and Doctor, D. H., 2014, Karst in the United States: A digital map compilation and database, U.S. Geological Survey Open-File Report 2014-1156, p. 23.

SUPPLEMENTAL MATERIAL

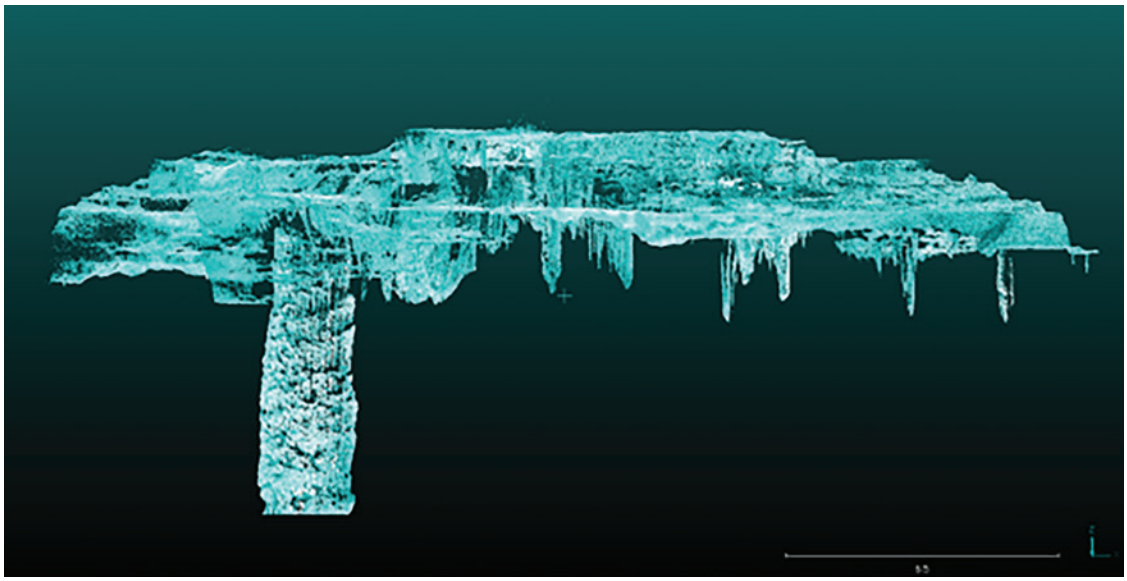


Figure S1. Side view of a large clip (24 × 9 m^2) of the Castle of the White Giants, containing very large and complex speleothems.

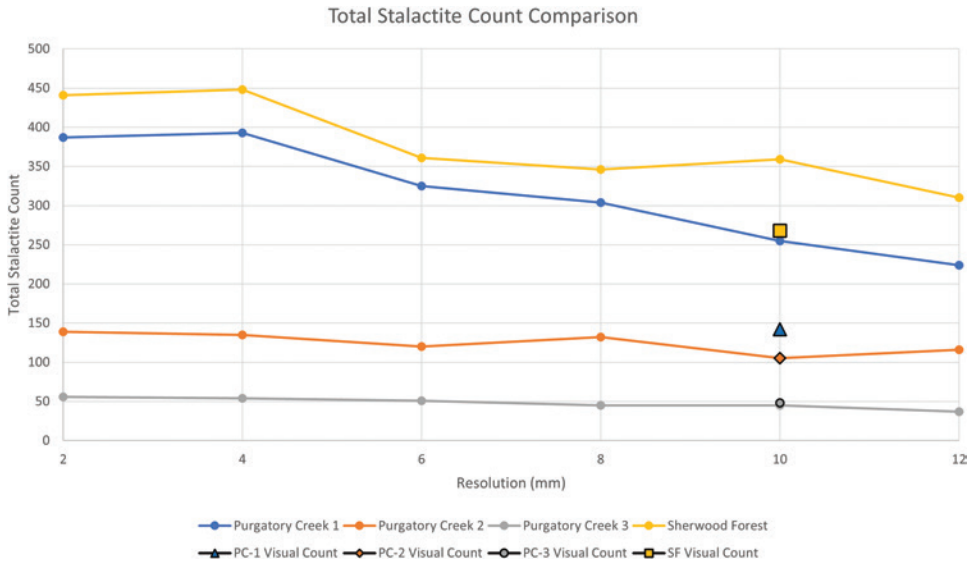


Figure S2. Graph showing total output stalactite counts at the tested resolutions compared to a manual count of the present stalactites. Total stalactite counts at Purgatory Creek section 1 and Sherwood Forest are significantly off from the manual counts, while Purgatory Creek section 2 and Purgatory Creek section 3 are most accurate.

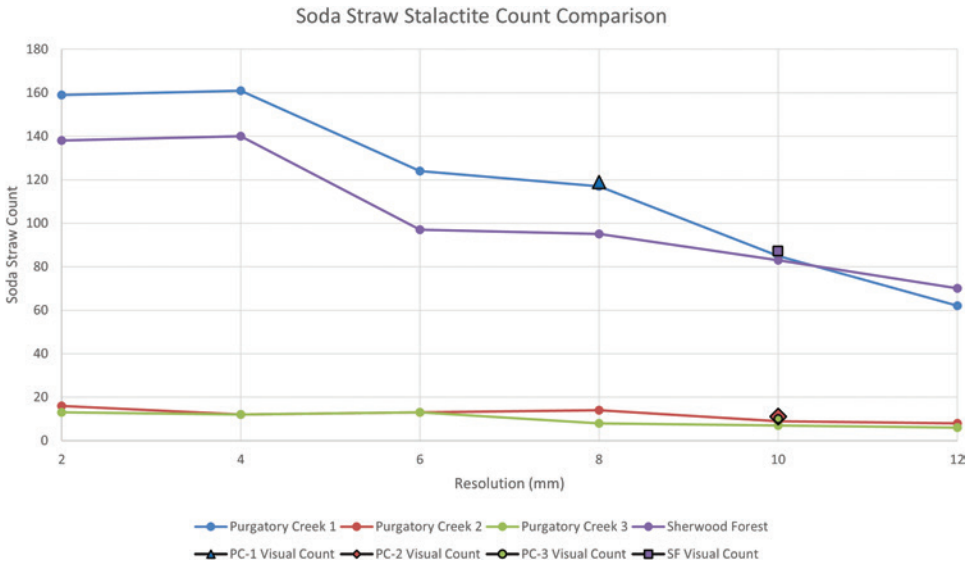


Figure S3. Graph showing output soda straw stalactite counts at the tested resolutions compared to a manual count of the present stalactites. Soda straw counts at Purgatory Creek section 1 are most accurate at 8 mm and Purgatory Creek section 2, Purgatory Creek section 3, and Sherwood Forest are most accurate at 10 mm.

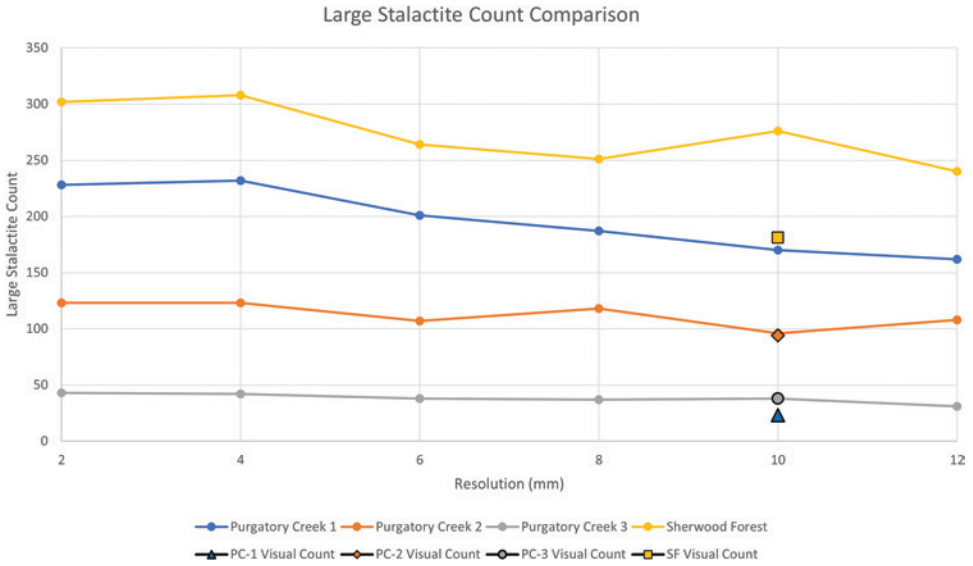


Figure S4. Graph showing output large stalactite counts at the tested resolutions compared to a manual count of the present stalactites. Large stalactite counts at Purgatory Creek section 1 and Sherwood Forest are significantly off from the manual counts, while Purgatory Creek section 2 and Purgatory Creek section 3 are most accurate at 10 mm.

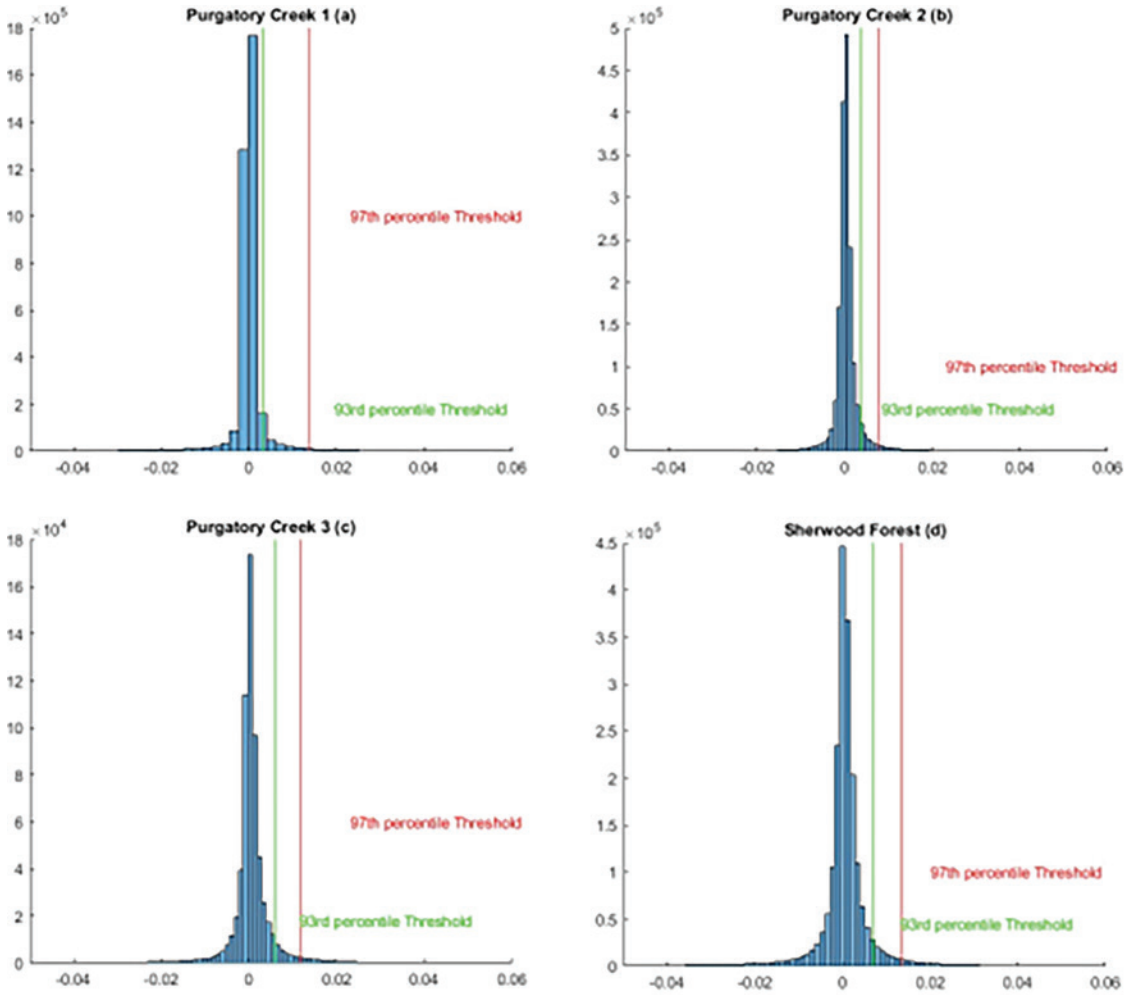


Figure S5. Histogram of anomalies and the thresholds used for stalactite (97th for stalactite identification and 93rd for flow identification) and flow type identifications of Purgatory Creek 1 (a), Purgatory Creek 2 (b), Purgatory Creek 3 (c), and Sherwood Forest (d).

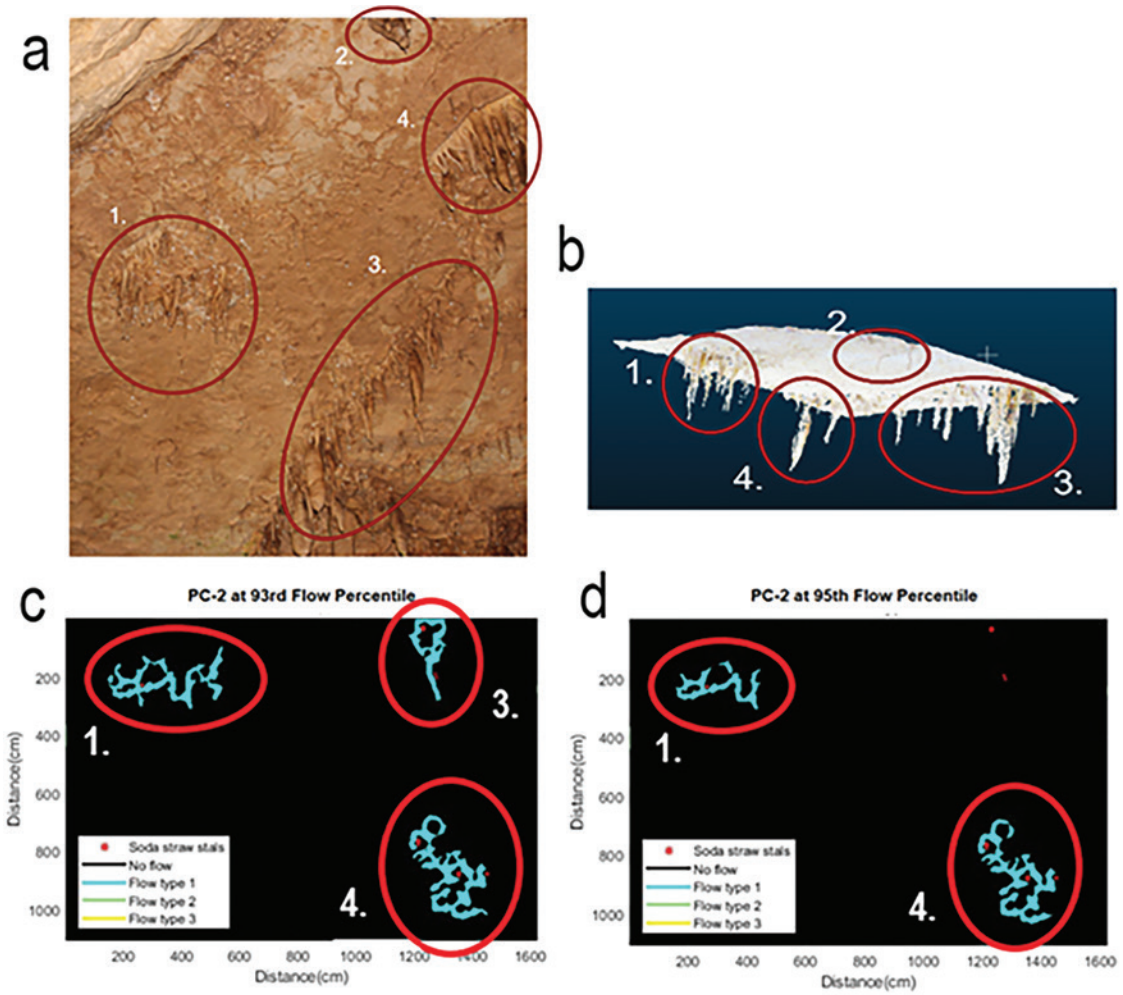


Figure S6. Comparison between flow threshold of a 93rd percentile shown in (c) and 95th percentile shown in (d) compared to a photo of Purgatory Creek 2 (a) and a LiDAR scan of the area (b) (same section used in Fig. 4).

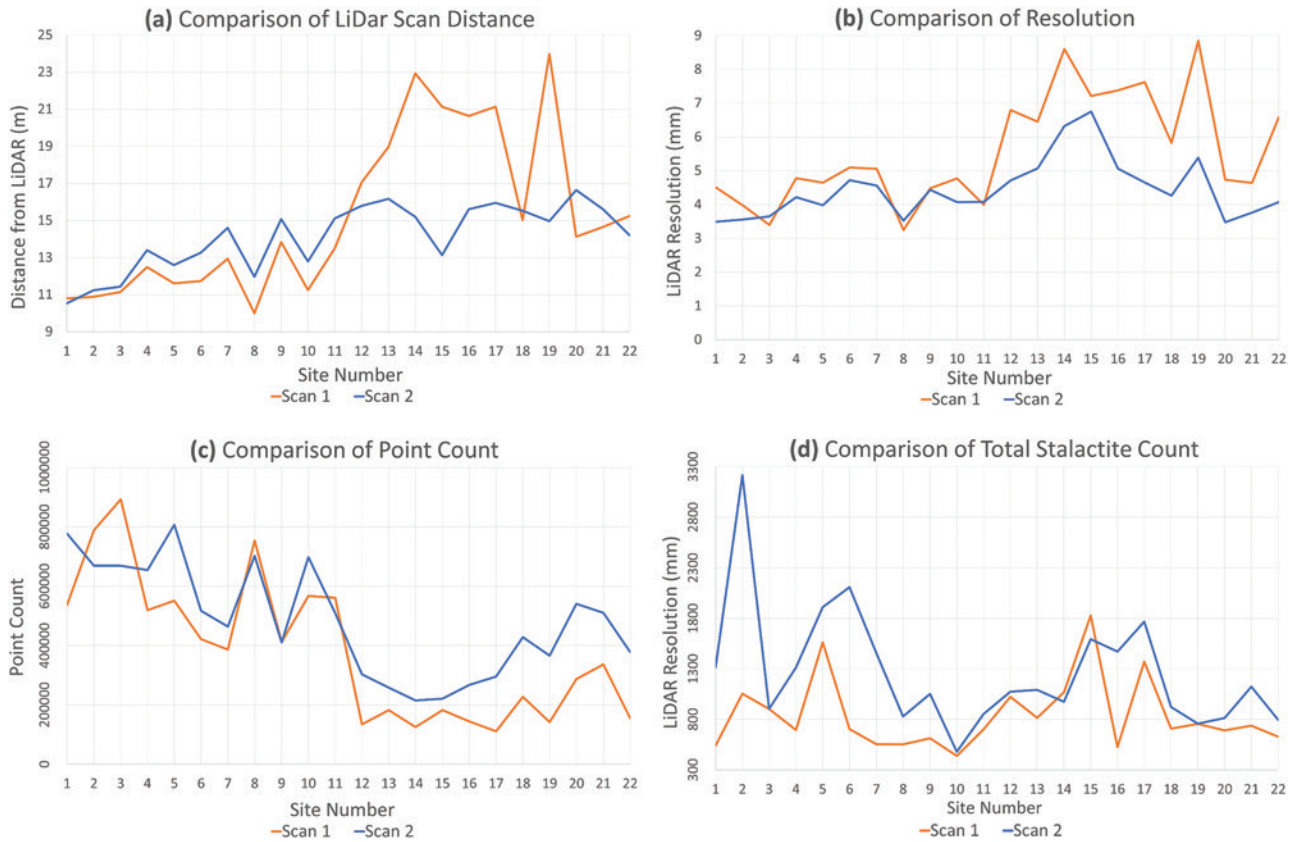


Figure S7. Graphs showing the differences in LiDAR scan distance (a), base point cloud resolution (b), point count of the individual clip locations (c), and total stalactite counts at each location between set 1 (represented by an orange line) with 7 scan locations and set 2 (represented by a blue line) with 14 scan locations (d).

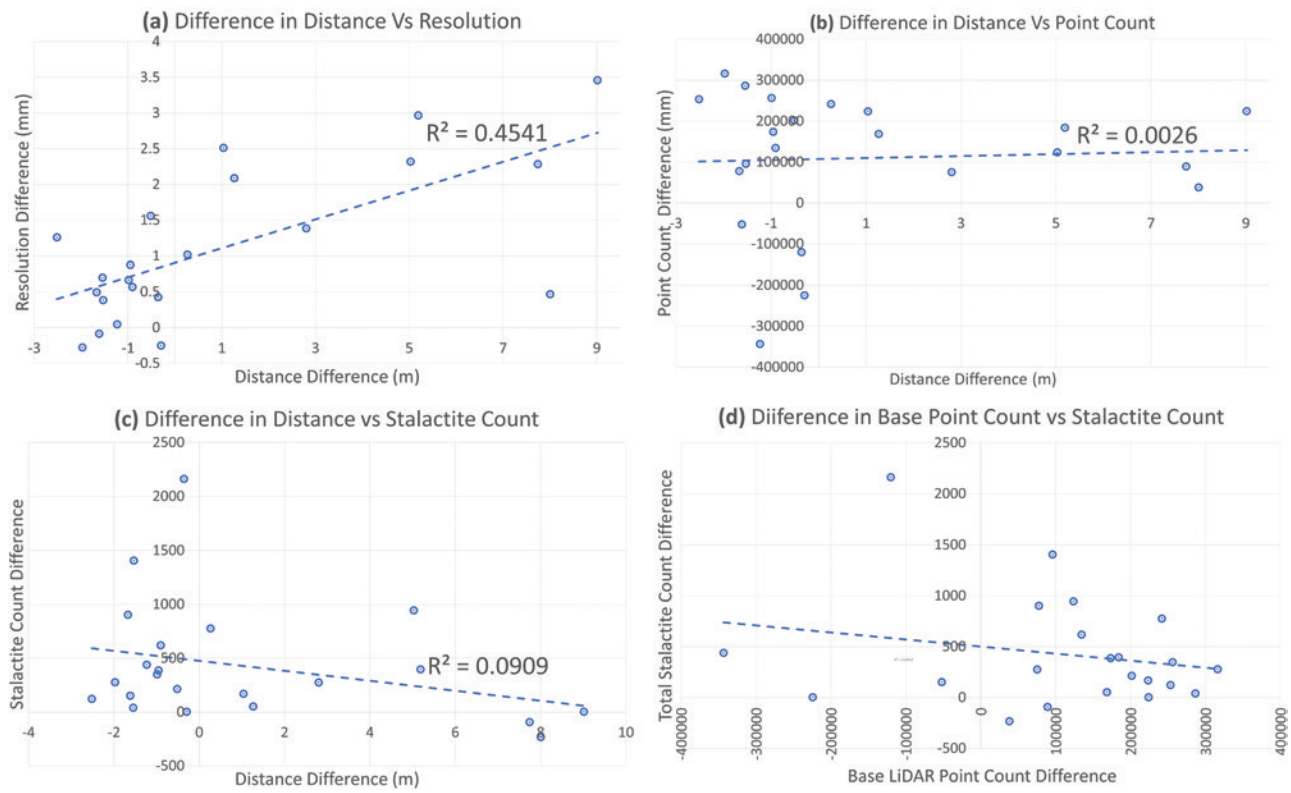


Figure S8. Plots showing the correlation between differences in scan distance and resolution (a), scan distance vs point count (b), scan distance vs stalactite count (c), and point count and stalactite count (d). R^2 values are listed in all subplots.

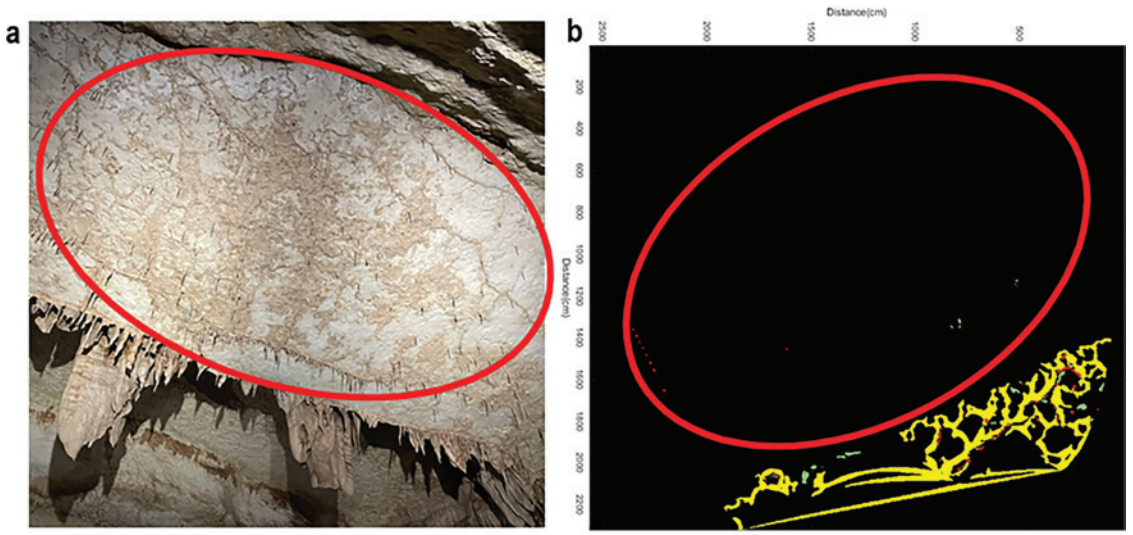


Figure S9. Comparison between an on-site photo of Purgatory Creek (a) and the final flow map of the area showing misidentification of soda straw locations (represented as red asterisk) from the center of the clip to the areas of cave ribbon.

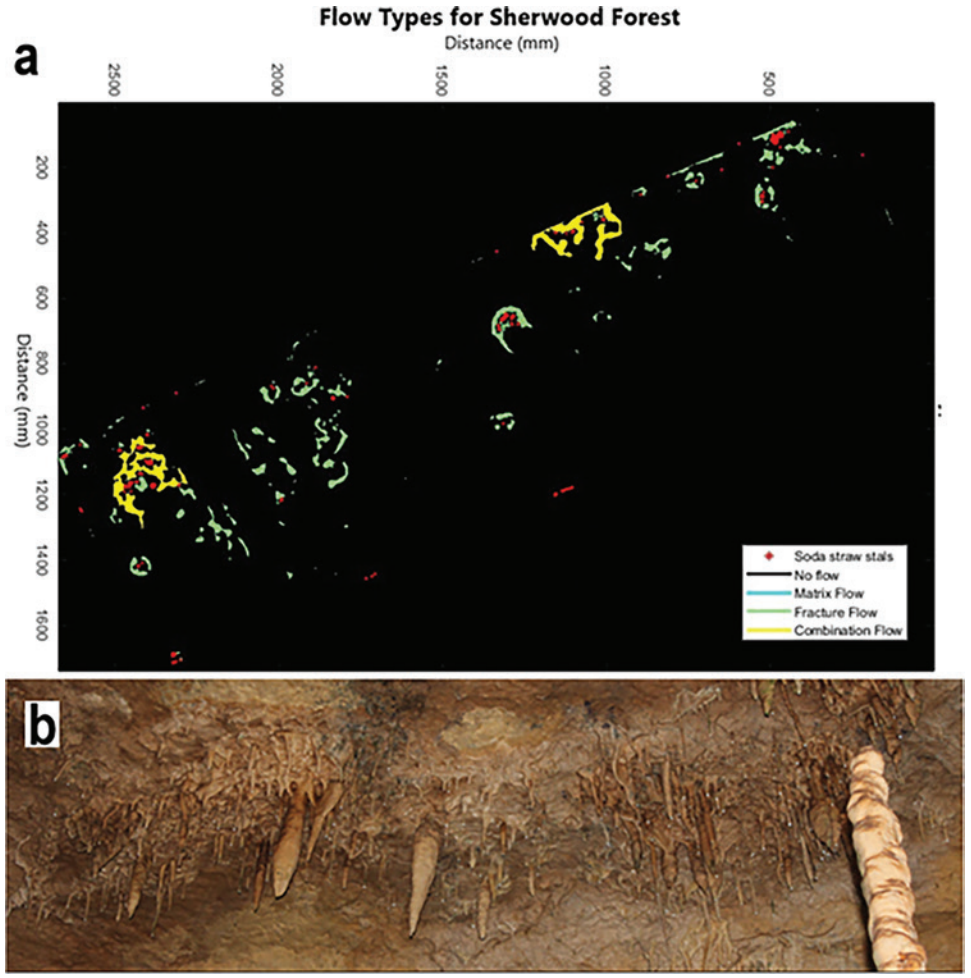


Figure S10. Comparison between an on-site photo of Sherwood Forest (a) and the final flow map (b) of the area showing more accurate identification of soda straw locations (represented as red asterisk).

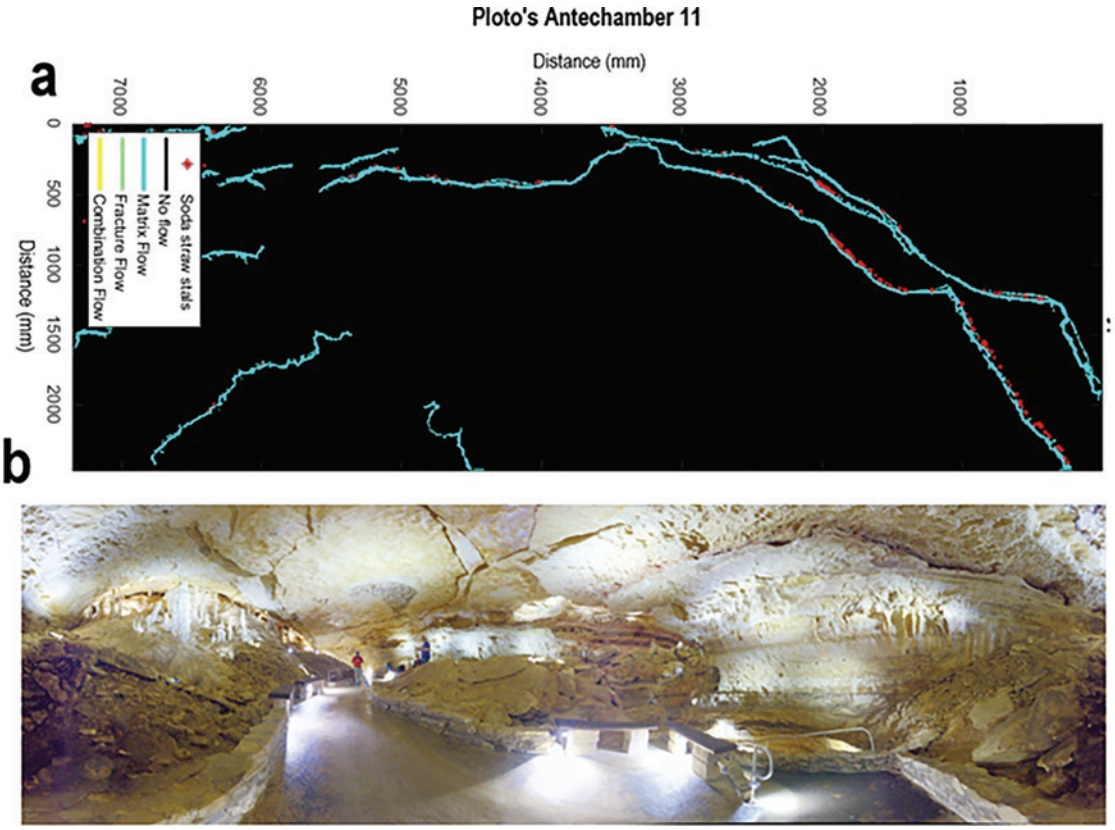


Figure S11. Comparison between LiDAR panoramic image and final flow map showing terracing with no stalactites identified as type 1 flow.